Report No. NAWCADWAR-95-12-TR

THE ANALYSIS OF A Z-FIBER REINFORCED PLATE

David John Barrett
Air Vehicle Engineering Department (Code 4331)
NAVAL AIR WARFARE CENTER AIRCRAFT DIVISION
P.O. Box 5152
Warminster, PA 18974-0591

11 SEPTEMBER 1995

FINAL REPORT
Period Covering October 1994 to September 1995

Prepared for
Air Vehicle Engineering Department (Code 4.3C)
NAVAL AIR WARFARE CENTER AIRCRAFT DIVISION
P.O. Box 5152
Warminster, PA 18974-0591

NOTICES

REPORT NUMBERING SYSTEM - The numbering of technical project reports issued by the Naval Air Warfare Center, Aircraft Division, Warminster is arranged for specific identification purposes. Each number consists of the Center acronym, the calendar year in which the number was assigned, the sequence number of the report within the specific calendar year, and the official 2-digit correspondence code of the Functional Department responsible for the report. For example: Report No. NAWCADWAR-95010-4.6 indicates the tenth Center report for the year 1995 and prepared by the Crew Systems Engineering Department. The numerical codes are as follows.

Code	Department
4.1	Systems Engineering Department
4.2	Cost Analysis Department
4.3	Air Vehicle Department
4.4	Propulsion and Power Department
4.5	Avionics Department
4.6	Crew Systems Engineering Department
4.10	Conc. Analy., Eval. and Plan (CAEP) Department

PRODUCT ENDORSEMENT - The discussion or instructions concerning commercial products herein do not constitute an endorsement by the Government nor do they convey or imply the license or right to use such products.

Reviewed By: _____ **Date:** 2 July 96
Author/COTR

Reviewed By: _____ **Date:** 6/24/96
LEVEL III Manager

DISCLAIMER NOTICE

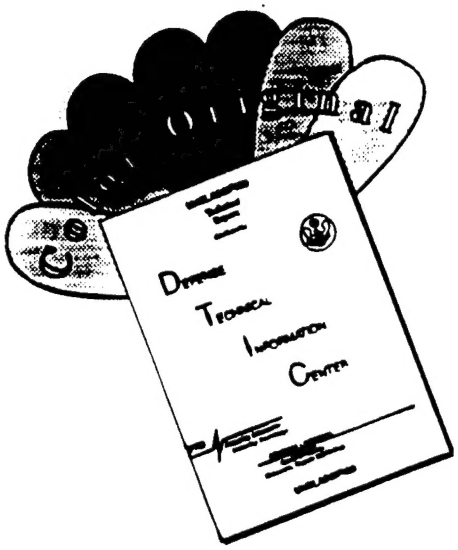

THIS DOCUMENT IS BEST QUALITY AVAILABLE. THE COPY FURNISHED TO DTIC CONTAINED A SIGNIFICANT NUMBER OF COLOR PAGES WHICH DO NOT REPRODUCE LEGIBLY ON BLACK AND WHITE MICROFICHE.

REPORT DOCUMENTATION PAGE

Form Approved
OMB No. 0704-0188

1. AGENCY USE ONLY *(Leave blank)*	2. REPORT DATE	3. REPORT TYPE AND DATES COVERED
	11 SEPT 95	FINAL REPORT OCT 94 TO SEPT 95

4. TITLE AND SUBTITLE

THE ANALYSIS OF A Z-FIBER REINFORCED PLATE

5. FUNDING NUMBERS

6. AUTHOR(S)

DAVID JOHN BARRETT

7. PERFORMING ORGANIZATION NAME(S) AND ADDRESS(ES)

Air Vehicle Engineering Department (Code 4331)
NAVAL AIR WARFARE CENTER; AIRCRAFT DIVISION
P.O. Box 5152
Warminster, PA 18974-0591

8. PERFORMING ORGANIZATION REPORT NUMBER

NAWCADWAR-95-12-TR

9. SPONSORING / MONITORING AGENCY NAME(S) AND ADDRESS(ES)

Air Vehicle Engineering Department (Code 4.3C)
NAVAL AIR WARFARE CENTER; AIRCRAFT DIVISION
P.O. Box 5152
Warminster, PA 18974-0591

10. SPONSORING / MONITORING AGENCY REPORT NUMBER

11. SUPPLEMENTARY NOTES

12a. DISTRIBUTION / AVAILABILITY STATEMENT

APPROVED FOR PUBLIC RELEASE; DISTRIBUTION IS UNLIMITED.

12b. DISTRIBUTION CODE

13. ABSTRACT *(Maximum 200 words)*

Z-fiber reinforcement is being examined for its ability to increase the through-the-thickness strength of advanced composite laminates, joints and structural interfaces. This report describes the results of an analysis effort that had the goal of developing an understanding of the mechanics of z-fiber reinforcement. Specific issues that were addressed in these analyses include thermal loadings, crack initiation, crack growth and load transfer.

14. SUBJECT TERMS

COMPOSITE STRUCTURES, THREE DIMENSIONAL COMPOSITES, Z-DIRECTION REINFORCEMENT

15. NUMBER OF PAGES

16. PRICE CODE

17. SECURITY CLASSIFICATION OF REPORT	18. SECURITY CLASSIFICATION OF THIS PAGE	19. SECURITY CLASSIFICATION OF ABSTRACT	20. LIMITATION OF ABSTRACT
UNCLASSIFIED	UNCLASSIFIED	UNCLASSIFIED	

TABLE OF CONTENTS

FIGURES

FIGURES (continued)

TABLES

1.0 INTRODUCTION

1.1 Purpose

Z-fiber reinforcement is being examined for its ability to increase the through-the-thickness strength of advanced composite laminates, joints and structural interfaces. If this technology proves successful, designers will be able to use it to help solve problems associated with cocured composite structure including skin-stiffener separation [1 & 2] and hat stiffener runout [3]. Also, it would find application in the development of damage tolerant skins [4 & 5], survivable composite wing structure [6] and unitized aircraft structure [7]. Obtaining a fundamental understanding of the interaction between the z-fiber reinforcement and the structure in which it is embedded is key to the development of this technology. To study this interaction, micromechanical stress analyses were performed based on the finite element method (FEM). The results of these analyses are reported herein.

1.2 Background

Laminated fiber reinforced materials have high in-plane strength to weight ratios. Because of this, they are the materials of choice for the construction of the wings and fuselage of fighter aircraft. A preferred form of laminated construction is integrally stiffened cocured structure because this method of fabrication reduces fabrication and assembly costs. The drawback to the use of laminates and of cocured structure is that laminates have poor through-the-thickness strength. Moderate out-of-plane loads can lead to delaminations, skin-stiffener separations and failed joints.

In an attempt to improve the through-the-thickness properties of laminates, researchers have examined the use of stitching, toughened resin systems and z-fiber reinforcement. Stitching involves the sewing of fibers through the thickness of laminates and through structural interfaces. The stitches directly resist pull-off loads and joint reactions. The drawbacks to stitching include a substantial capital investment, a degradation of laminate in-plane strength and stiffness properties, and labor intensive construction procedures for large structural parts. In toughened resin systems, the formulation of the resin is changed in order to improve the through-the-thickness

structural properties. Toughened resin systems, however, are costly and still do not provide adequate fracture toughness. Z-fiber reinforcement involves the direct insertion of reinforcing fibers in the through-the-thickness direction of laminates and structural interfaces. (In analytical models, the through-the-thickness coordinate line is usually designated the "z-axis". The term "z-fibers" derives from the orientation of the z-fibers along this axis.) At this point in time, z-fiber reinforcement appears to offer many benefits.

The z-fiber reinforcement process was developed by Foster-Miller, Inc. of Waltham, Massachusetts. Their efforts were funded by in-house investment and through various Small Business Innovative Research programs (SBIR). Recently, Foster-Miller announced the formation of Aztex, Inc.; a majority owned subsidiary of the parent company. Aztex will serve as the supplier of z-fiber products, equipment and engineering services.

The typical z-fiber reinforcing process [8] starts by placing a release film, a z-fiber preform and a rigid tool onto a laid-up prepreg laminate. The z-fiber preform consists of a structural foam that contains the reinforcing fibers. The part is then vacuum bagged and processed using a standard autoclave cure cycle. The heat softens the preform which collapses under the applied pressure. The z-fiber reinforcement is thereby driven into the laminate. (The foam is chosen for its ability to provide lateral support to the fibers during the insertion process.) Upon removal from the autoclave, the compacted foam is removed and discarded. The process is completed with the removal of any pin material that projects above the laminate.

Z-fiber preforms are made with a specially designed insertion machine that embeds the reinforcing fibers into a structural foam. The insertion machine can be programmed to insert the z-fibers to various lengths, spacing and patterns [9]. Preforms are available in a variety of thicknesses that range from 1 mm to 19 mm for single fiber insertions and up to 51 mm for multiple fiber insertions. The maximum areal densities are 1% for standard tape, 3% for standard fabric and 7.5% for modified fabric. A number of different reinforcing materials are in use including pan and pitched based carbon/epoxy, carbon bismaleimides, glass/epoxy, titanium, refractory alloys and stainless steel. The diameters of the reinforcing fibers range from 0.15 mm to 1 mm.

The types of prepreg systems to which z-fiber reinforcement is applied include AS4/3501-6, IM7/8551-7, PEEK/APC-2, and S-2(glass)/polyester. Consolidated thermoplastics have also been reinforced with an ultrasonic insertion method.

Foster-Miller claims that the z-fibers benignly penetrate laminations when proper processing procedures are employed. There is minimal fiber breakage. This claim is supported by photomicrographs that show that the ply fibers, that were originally in the path of the penetrating z-fibers, gently bend around the z-fibers. This displacement of the fibers results in the formation of elliptically shaped resin pools (see Figure 1). On the minor axis of these ellipses, the ply fibers are in close proximity to the z-fibers. Along the major axis, the resin pool can extend for several z-fiber radii. The orientations of the ellipses change from ply to ply as the individual ply orientations change.

Test results [9] indicate that z-fiber reinforcement leads to an 18 fold increase in Mode I fracture toughness. (The definition of this material property does not strictly apply to crack growth in z-fiber reinforced laminates. The test results must be interpreted on a structural level as opposed to a material level.) The use of z-fiber reinforcement also leads to a 50% increase in compression after impact strength over unreinforced laminates. Reinforced laminates do not experience any decrease in compression strength and retain from 91 to 98% of their unreinforced tensile strength and modulus. A 50% improvement in ultimate stiffener pull-off loads has been recorded.

A substantial SBIR investment has been made in z-fiber technology. Although some of this money was used to support process development, a large portion of it was used to develop and test various structural configurations. Currently, two large scale technology development programs are making use of z-fiber reinforcement; Lockheed's "Robust Composite Sandwich Structures" program and McDonnell-Douglas's "Advanced Lightweight Aircraft Fuselage Structures" program [7]. The emphasis of these programs is on the demonstration of new structural technologies. These two programs and the SBIR efforts do not include tasks to investigate the fundamental mechanical behavior of z-fibers. A future Great Lakes Composite Consortium (GLCC) program, directed specifically at the development of z-fiber reinforcement technology, will include an emphasis on engineering

science. However, early feed back from the prime airframers shows that they will be vying for making and testing the structural parts that give them their greatest concerns.

What is missing in these research and development activities is a basic investigation of how the z-fibers interact with the structure in which they are embedded. The success of this technology is dependent on a clear understanding of the mechanics of this interaction.

In a typical aircraft stress analysis that is based on the finite element method, the resolution of the models is rarely finer than the skin thicknesses or the individual ply thicknesses. The mechanics of z-fiber reinforcement has been examined to this level by Foster-Miller. Proposals to the GLCC program are expected to include the same kind of modeling with individual fibers represented by single finite elements. At this point, the suspicion is that these models will not be able to fully characterize the interaction between the z-fiber and the laminate. If the stress transfer between the z-fibers and the surrounding structure follows a shear lag type of distribution, then highly local stress concentrations will develop around the z-fibers at any free boundary. The characteristic dimension of these stress concentrations is expected to be less than a typical ply thickness. Therefore the proposed level of finite element modeling will not be able to resolve the magnitude and distribution of these stress concentrations. However, it is this type of information that will be critical to the development of the optimum form and usage of z-fiber reinforcement.

To address this issue, the Strength Branch of the Naval Air Warfare Center - Aircraft Division, Warminster (NAWCADWAR), under the sponsorship of the Office of Naval Research, undertook an effort to examine the stress fields that are generated in laminates by the introduction of z-fibers. The approach was based on the development of finite element models that have a fine enough resolution to examine stress concentrations about the z-fibers. In addition, less refined models were used to examine the effect of z-fibers on crack tip stress fields.

2.0 ANALYSIS

2.1 Problem Descriptions

Two types of structural problems were addressed. The first involved the application of thermal loads to z-fiber reinforced plates. The second examined the effect of z-fibers on crack initiation and growth.

Thermal stresses are generated when materials with different coefficients of thermal expansion (COTE) are constrained to respond in unison to thermal loads. In general, the COTE of z-fibers and of the laminates in which they are embedded are different. Thus, both in-plane and through-the-thickness stresses are generated when z-fiber reinforced laminates experience a change in temperature. The magnitude and distribution of these stresses are of concern for thermal fatigue and for overloads resulting from thermal loads acting in conjunction with mechanical loads.

Z-fiber reinforcement can also affect the growth and development of in-plane cracks. For crack initiation, the z-fibers can help to shield the laminate interfaces from damaging stresses. Also, when in-plane cracks have penetrated throughout a region that contains an intact z-fiber, the z-fiber can transmit loads between the separated crack surfaces. This will reduce the stresses at the tips of the crack and will arrest the crack growth. To produce these benefits, the z-fibers receive load from the laminate through interfacial shear stresses. These stresses, which will be concentrated around the z-fibers in the vicinity of the separated surfaces, can introduce new failure modes (e.g., through-the-thickness cracks, fiber slippage, surface cracks, etc.).

To examine the thermal load and the crack stress issues, a z-fiber reinforced plate was analyzed. The plate consisted of an 18 ply quasi-isotropic lamination of AS4/3501-6. The z-fibers were taken to be T300/5208 circular pins with a diameter of .280 mm. Table 1 lists the mechanical properties of these materials as well as those of pure resin and titanium. The total plate thickness was 3.50 mm. The areal density of the z-fibers was .5%, with the z-pins arranged in a square array with a spacing of 3.50 mm.

The z-fiber reinforced plate was analyzed using the axisymmetric and the three-dimensional stress models shown in Figure 2.

2.2 Axisymmetric Stress Model

In the axisymmetric model, a single z-fiber, the surrounding resin pool and the laminate were modeled as three concentric cylinders. The radius of the model was 1.75 mm which is half the distance to the adjacent z-fibers. The resin pool was assumed to have a thickness of .030 mm.

Two assumptions are implicit in this model. The first is that the individual ply orientations are not critical to the stresses of concern (the through-the-thickness normal and shear stresses). Based on this, the laminate was treated as a monolithic quasi-isotropic material. The second assumption is that the interfacial stresses between the z-fiber and the surrounding resin pool are relatively insensitive to the pool thickness. Therefore a circular pool, uniform throughout the thickness, was used to represent an elliptically shaped pool whose major axis changes orientation with each change in ply direction. (Subsequent work will be needed to validate this last assumption. The work reported here is a reasonable attempt to determine the mechanical response.)

The axisymmetric model was used to examine the thermal stresses that are induced by a uniform temperature change in the plate. Also, it was used to determine the axisymmetric crack tip stresses that form in a region about a z-fiber under a uniform through-the-thickness crack opening load (see Figure 3). Because the model and the applied loads were axisymmetric, the model was analyzed with a two-dimensional axisymmetric finite element mesh (see Figure 4). The mid-plane symmetry of the plate was used to reduce the size of this mesh. (The mesh extends from the mid-depth to the surface of the plate.) Figure 4 shows the X-coordinate line extending from the centerline of the z-fiber into the radial direction. The Y-coordinate extends from the mid-depth of the plate into the axial direction of the z-fiber. The notation on this figure indicates the location of the z-fiber (MP=1), the resin (MP=2) and laminate (MP=3). The mesh density was sized to analyze the stress concentration that would occur in the interfacial area between the z-fiber and the resin when thermal loads are applied. An enlarged view of the interfacial area at the surface of the model is shown in Figure 5. The aspect ratios of the elements have an upper limit of approximately 3 to 1.

2.2.1 Thermal Stress Analysis

Figures 6 and 7 show the displacements that occur in the axisymmetric finite element mesh for a 10 °C rise in temperature. Numerical values for the radial (Disp_X) and axial (Disp_Y) displacements are shown in Figures 8 and 9. The displacements in the axial direction on the outer edge of the model match the displacements that would be found for the general laminate. This establishes the validity of using the model to analyze the thermal behavior of the plate. The displacements of the z-fiber at the surface of the model are approximately the value predicted by a Rule-of-Mixtures model. The radial displacements in the z-fiber are seen to be negative. This is caused by the particular combination of materials used in this model. The laminate, which has a high in-plane modulus and a low COTE, acts as a barrier to the thermal radial growth of the z-fiber and the resin. The combination of the moduli and the COTE of the resin dominates the corresponding in-plane properties of the z-fiber. The result is that the resin pushes inwards from the laminate into the z-fiber. The displacement plots also show the intense shearing that occurs near the model's upper surface in the elements that are used to model the resin pool.

The through-the-thickness normal stresses (Sigma_Y) are shown in Figures 10 and 11. The stresses in the z-fiber are tensile since the laminate's greater thermal growth pulls on the z-fiber. On the other hand, the stresses in the laminate are compressive since the z-fiber retards the laminate's thermal movements. The laminate's compressive stresses tend to zero along the radial coordinate.

The radial stresses (Sigma_X) are shown in Figures 12 and 13. As the radial displacement field indicates, the radial stresses in the z-fiber, the resin pool and the adjacent laminate are compressive. The radial stresses in the laminate tend to zero in the radial direction. The hoop stresses (Sigma_Z) are shown in Figures 14 and 15. These stresses are compressive in the z-fiber and in the resin pool but become tensile in the adjacent laminate. The hoop stress also tends to zero in the radial direction. Figures 13 and 15 show how the stresses deviate from these patterns because of the free surface.

The through-the-thickness shear stresses are shown in Figures 16 and 17. The highly stressed area is seen to occur in the interface between the z-fiber and the resin pool just below the free boundary.

2.2.2 Axisymmetric Crack Tip Stress Analysis

A crack was introduced at mid-depth in the axisymmetric model. The crack penetrated from the outer rim of the model inwards along the radial direction (see Figure 3). The crack was introduced into the finite element mesh by releasing the restraints against the Y-direction displacements along the base of the mesh. Figure 18 shows the mesh and the boundary conditions for a crack that has penetrated to a radial location of .700 mm, that is, to within 2 z-fiber diameters of the face of the z-fiber.

Figure 19 shows the displacements that occur in the mesh for crack opening loads applied around the rim of the model (18 nodal forces of .001N acting in the vertical direction (see Figure 18)). Figures 20 through 23 show the associated stress fields.

As a basis for comparison, the axisymmetric model was used to analyze a section of laminate that contains no z-fiber reinforcement. For this case, the parts of the mesh, that were previously used to represent the z-fiber and the resin pool, were reassigned the material properties of the laminate. The crack opening loads and the displacement boundary conditions remained the same. The resulting displacement field is shown in Figure 24. The through-the-thickness normal stresses are shown in Figure 25. The stress components in the element at the tip of the crack for the reinforced and unreinforced cases are listed and compared in Table 2. A comparison between the through-the-thickness stresses that occur along the mid-plane of the reinforced (Series 1) and the unreinforced (Series 2) cases is shown in Figure 26.

The final analysis performed on the axisymmetric model considered a crack that had penetrated up to the face of the z-fiber. The crack opening loads remained the same. The resulting displacements are shown in Figure 27. The stress fields are shown in Figures 28 and 29.

2.3 Three Dimensional Stress Model

Mode I crack opening loads were applied along the entire edge of the plate from which the three-dimensional stress model was taken. A mid-plane crack on this edge was

assumed to extend inwards to a point midway between the first and second z-fiber (see Figure 30). Given the scale of the z-fiber spacing, the mechanical response to the described load in each row of z-fibers will be approximately the same. (The only exception would be for rows near the unloaded lateral edges, the analysis of which is not addressed here).

To analyze the stresses in the crack tip, a three-dimensional stress model was formulated which consisted of a rectangular block of laminate containing two z-fibers (see Figures 2 and 30). The block was taken from the loaded end of the plate with the long edge of the block directed towards the plate's interior. The width of the block was 3.50 mm and its' length was 7.00 mm. The z-fibers were located along the widthwise centerline of the block with the z-fibers centered 1.75 mm from the front and back faces of the block. As defined, the model has two planes of structural symmetry. Since the crack tip stresses were of interest, the pools of resin about the z-fibers were not included in the model.

To achieve the quasi-plane strain conditions that exist between the rows of z-fibers, the out-of-plane displacements on the side faces of the model were held fixed. At the rear of the model, the displacements were assumed to be free of any restraint. Implicit in this assumption is that the stiffness of the plate past the second z-fiber has a negligible affect on the crack tip stresses.

The three-dimensional model was analyzed with a mesh of 8 noded isoparametric solid elements. Because the structure and the loading were symmetric about the mid-plane of the plate and about a vertical plane through the centers of the two z-fibers, only the upper right hand quarter of the stress model was analyzed. Figure 31 shows the mesh with the origin of the reference coordinate system located at the point where the two planes of structural symmetry intersect the plane perpendicular to the tip of the crack. The X-coordinate line of this system extends towards the free edge of the plate, the Z-coordinate line extends upwards through the thickness of the plate, and the Y coordinate line completes a right handed coordinate system. The notation on Figure 31 indicates the location of the z-fiber (MP=1) and the laminate (MP=2).

The intention of the analysis was to examine the effect that z-fibers have on crack propagation. This was accomplish by comparing a case in which the z-fiber remains intact

in the cracked region against a case were the z-fiber is severed in the plane of the crack. Mechanically, the last case is equivalent to no reinforcement being present at all. The boundary conditions used in the first case are shown in Figures 32 and 33. Note that the intact z-fiber was modeled by fixing the displacements in the plane of the crack. The right hand side of Figure 32 shows the applied pressure (1 MPa). The boundary conditions in the second case were identical to the first with the exception that the z-fiber displacements were released at the crack (see Figure 34). For making this comparison, the exact level of stress concentration about the tip of the crack was not needed so that the three dimensional mesh used here is not as refined as the axisymmetric mesh.

2.3.1 Crack Tip Stress Analysis

Figure 35 shows the displacements that occur when the crack opening loads are applied and the z-fiber remains intact. Figures 36 and 37 show different views of this displacement field. The associated bending stresses (Sigma_X), the through-the thickness normal stresses (Sigma_Y), the in-plane lateral stresses (Sigma_Z) and the shear stresses (Tau_XZ) are shown in Figures 38 through 41. The tractions at the rear of the model are negligible, which validates the assumption to neglect the stiffness of the adjacent laminate. The displacements and stresses for when the z-fiber was severed are shown in Figures 42 through 47. A comparison between the two cases for the peak stresses at the tip of the crack is made in Table 3.

3.0 CLOSURE

3.1 Discussion and Conclusions

In the thermal stress analysis it was shown that thermal loads lead to stress concentrations in an AS4/3501-6 laminate reinforced with T-300 z-fibers. The maximum shear stress in the interfacial resin was shown to be 3.52 MPa for a temperature rise of 10 °C (see Figure 16). Since an aircraft component can routinely experience temperature changes of 50 to 60 degrees and since a typical resin has a shear strength of 60 MPa, the predicted thermal stress concentrations are not negligible.

Matching the COTE of the z-fibers to that of the laminate will help to control the thermally induced shear stresses. For instance, titanium would be a better candidate for reinforcing an AS4/3501-6 laminate since its COTE is higher than that of T-300. Note however, that this higher COTE and titanium's large elastic modulus may lead to the build-up of in-plane stresses. Therefore, unless the materials of construction are perfectly matched, thermal stresses, thermal cycling and thermal fatigue are of concern. These issues should be addressed in the environmental test plans of all of those who are evaluating the use of this technology.

The stress analyses showed that the z-fibers resist through-the-thickness loads only when those loads are applied in the immediate vicinity of a z-fiber (see Figure 26 and Table 2). This means that, for typical z-fiber areal densities, most of a laminate will remain unprotected from through-the-thickness loads. Therefore z-fibers can do very little to prevent crack initiation.

Once an in-plane crack has propagated throughout a region that contains an intact z-fiber, the z-fiber will pick-up the through-the-thickness loads. This will greatly reduce the stresses at the tip of the crack (see Table 3 and compare Figures 39 and 45). Therefore z-fibers have a significant affect on crack propagation.

When z-fibers resist through-the-thickness stresses, there is a shear lag type of stress transfer between the z-fiber and the surrounding material (see Figure 29). The magnitude of this stress concentration needs to be determined in order to avoid unexpected failure modes and to achieve an optimized design.

The characteristic dimension of the stress concentrations examined in this work are less than the individual composite ply thicknesses. Aircraft analysts rarely develop stress models as fine as ply thicknesses. Therefore current modeling methods will not be able to predict the local effects of z-fiber usage. Also, in order to avoid computational expense, there is a need to develop a micromechanical model that can bridge the gap between the typical aircraft stress analysis and the refined FEM meshes presented in this work.

4.0 REFERENCES

1. Renieri, M. P. and Garrett, R. A., "Stiffener/Skin Interface Design Improvements for Postbuckled Composite Shear Panels," Report No. NADC-80134-60, April 1982.
2. Tsai, H. C., "Solution Method for Stiffener-Skin Separation in Composite Tension Field Panel," Report. No. NADC-82171-60, October 1982.
3. "Improved Hat Development," Northrop Corporation Aircraft Division F/A-18 Oversite Review, August 8, 1994.
4. Dardzinski, P., "Ice Impact Resistance of Thin Skin Composite Laminates," Foster-Miller Inc. Report No. NAV-1150-FM-94218-882, July 1995.
5. Yen , C. and Chatterjee, S. N., "Ice Impact for Thin Skin Composite Laminates," Material Sciences Report No. 3512/AA17, August 1995.
6. Horton, R. A., "The JTCG/AS Vulnerability Reduction Subgroup," *Aircraft Survivability*, Summer 1994, pp. 6-9.
7. "Advanced Lightweight Aircraft Fuselage Structure (ALAFS) Program," McDonnell Douglas Aerospace Corporation Quarterly Reports, Contract N00019-91-G-0091, 1995.
8. Freitas, G., Magee, C., Dardzinski, P. and Fusco, T., "Fiber Insertion Process for Improved Damage Tolerance in Aircraft Laminates," Journal of Advanced Materials, July 1994.
9. Altergott, W., "The Z-Fiber Process, Through Thickness Reinforcement for Composite Structures," Proceedings of the Tenth DOD/NASA/FAA Conference on Fibrous Composites in Structural Design, NAWCADWAR-94096-60, 1994, pp. 71-93.

T300/5208 Z-Fiber (Transversely Isotropic)

Axial Modulus	152. GPa
Transverse Modulus	10.3 GPa
Axial Poisson's Ratio	0.31
Axial Shear Modulus	5.70 GPa
Transverse Shear Modulus	3.60 GPa
Axial COTE	0.54 με/°C
Transverse COTE	19.8 με/°C

Resin (Isotropic)

Extensional Modulus	3.52 GPa
Poisson's Ratio	0.38
Shear Modulus	1.28 GPa
COTE	67.9 με/°C
Tensile Strength	40 MPa
Compressive Strength	69 MPa
Shear Strength	60 MPa

AS4/3501-6 Laminate (Quasi-Isotropic)

In-Plane Modulus	54.3 GPa
Through-the-Thickness Modulus	10.6 GPa
Through-the-Thickness Poisson's Ratio	.0508
In-Plane Shear Modulus	3.45 GPa
Through-the-Thickness Shear Modulus	20.7 GPa
In-Plane COTE	1.93με/°C
Through-the Thickness COTE	32.0 με/°C

Titanium (Isotropic)

Extensional Modulus	110. GPa
Poisson's Ratio	0.30
Shear Modulus	4.34 GPa
COTE	8.82 με/°C

Table #1 Material Properties

Stress Component	Unreinforced Laminate (MPa)	Reinforced Laminate (MPa)	Reduction of Stress (%)
σ_{xx}	.174	.162	6.9
σ_{yy}	.169	.155	8.3
σ_{zz}	.158	.152	3.9
σ_{xy}	-0.14	-.013	6.6
First Principal	.185	.172	7.0
Second Principal	.158	.152	3.8
Third Principal	.158	.146	7.6

Table #2 Reduction of Stress due to the Presence of a Z-Fiber

Stress Component	Severed Z-Fiber (MPa)	Intact Z-Fiber (MPa)	Reduction of Stress (%)
σ_{xx}	23.7	7.74	67
σ_{yy}	10.3	2.78	73
σ_{zz}	11.5	2.49	78
σ_{xy}	-	-	-
σ_{xz}	1.25	.151	88
σ_{yz}	-	-	-

Table #3 Reduction in Nodal Stress due to Intact Z-Fiber

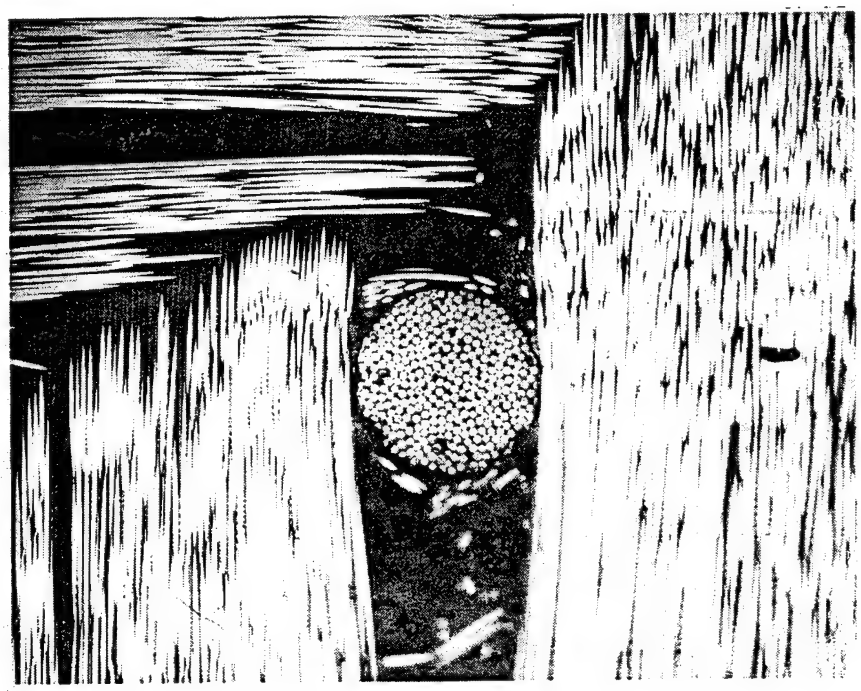

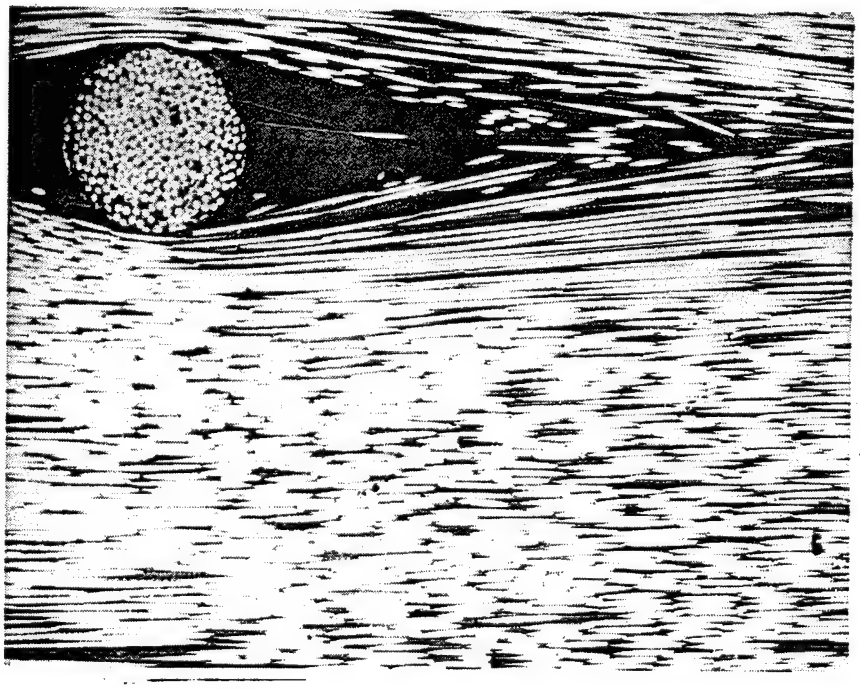

Figure 1. — Photomicrographs of Z-Fiber Reinforced Laminate (160×)

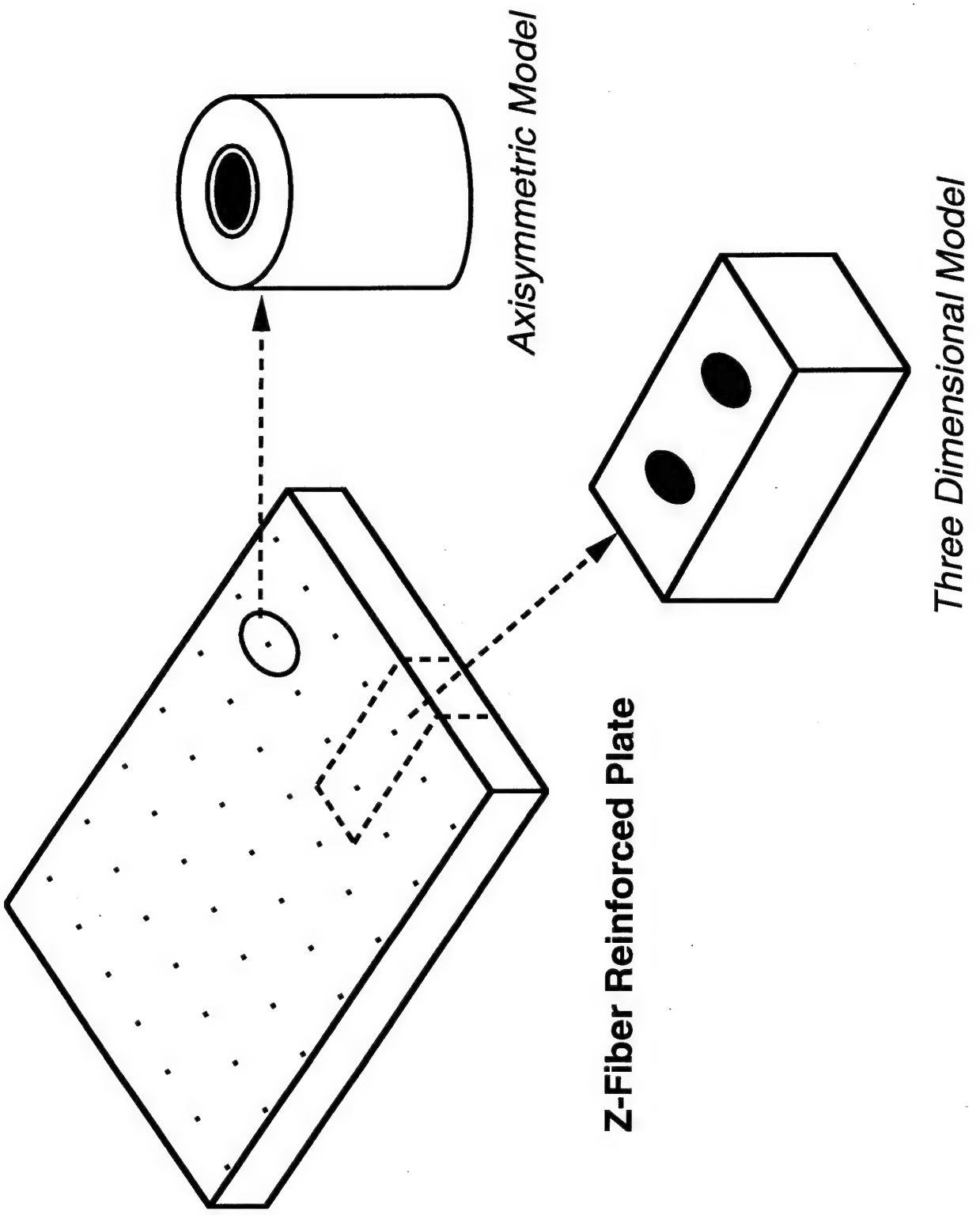

Figure 2 — Stress Models

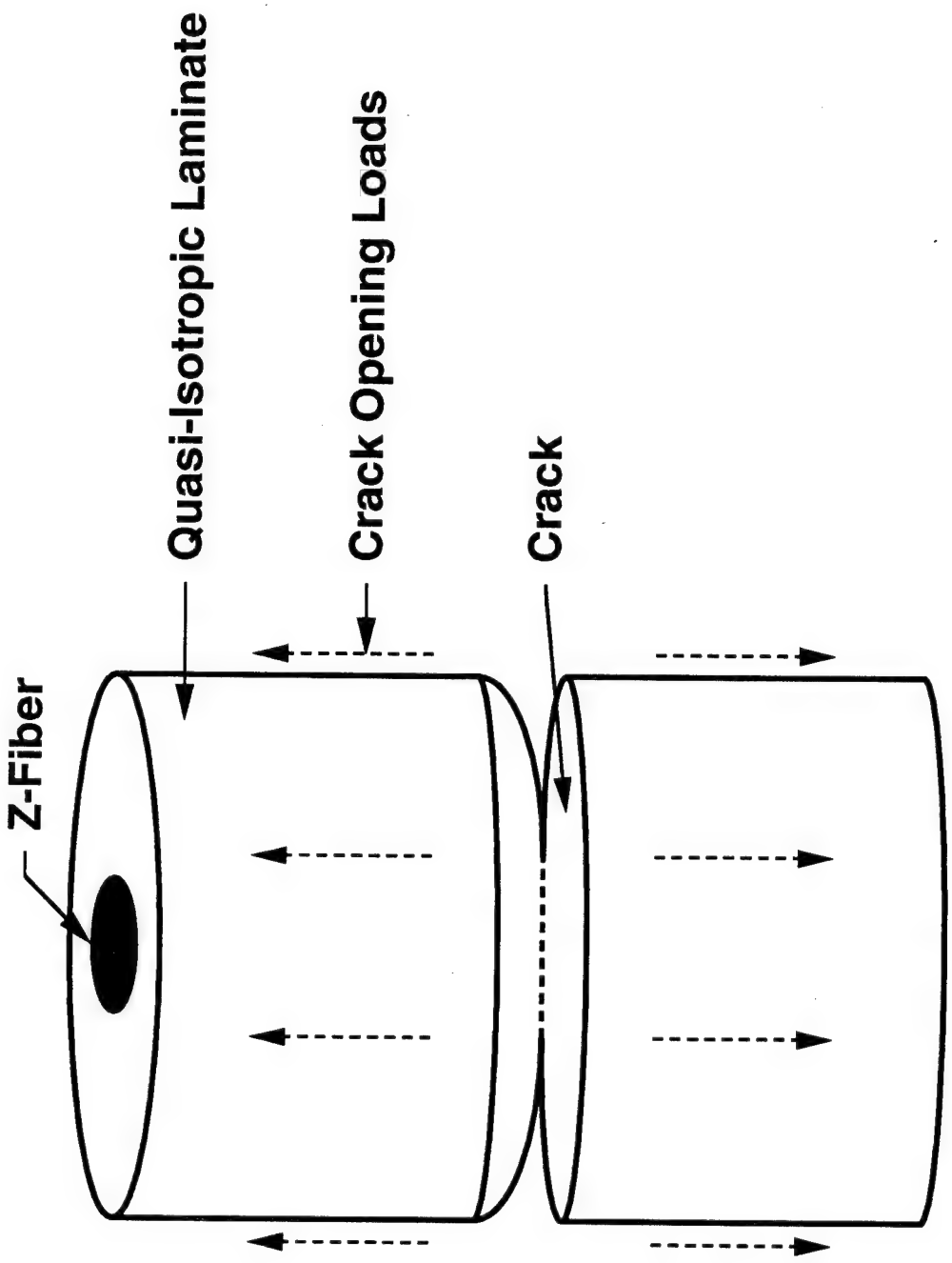

Figure 3 — Axisymmetric Crack Tip Problem

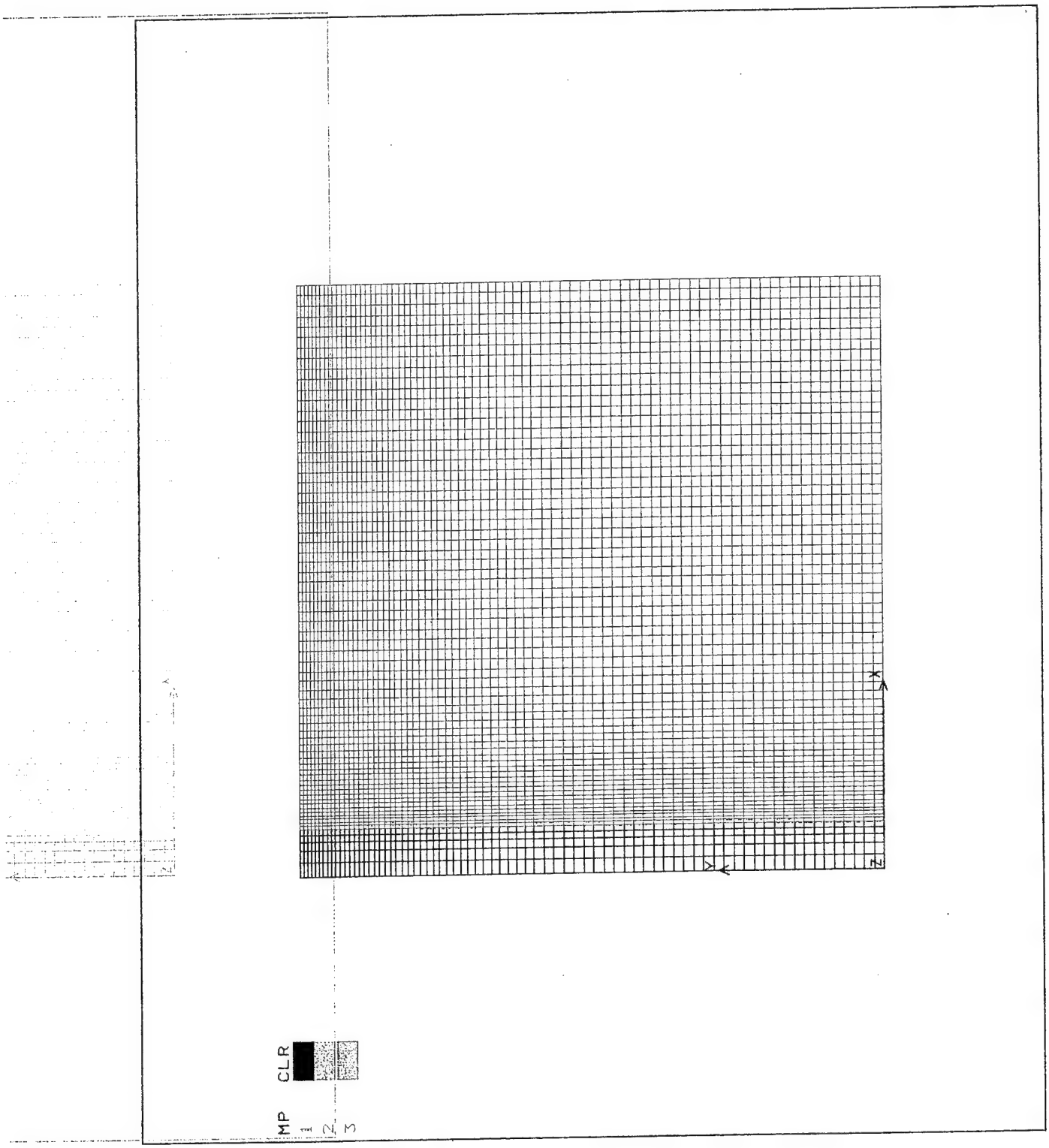

Figure 4 — Two Dimensional Axisymmetric Finite Element Mesh

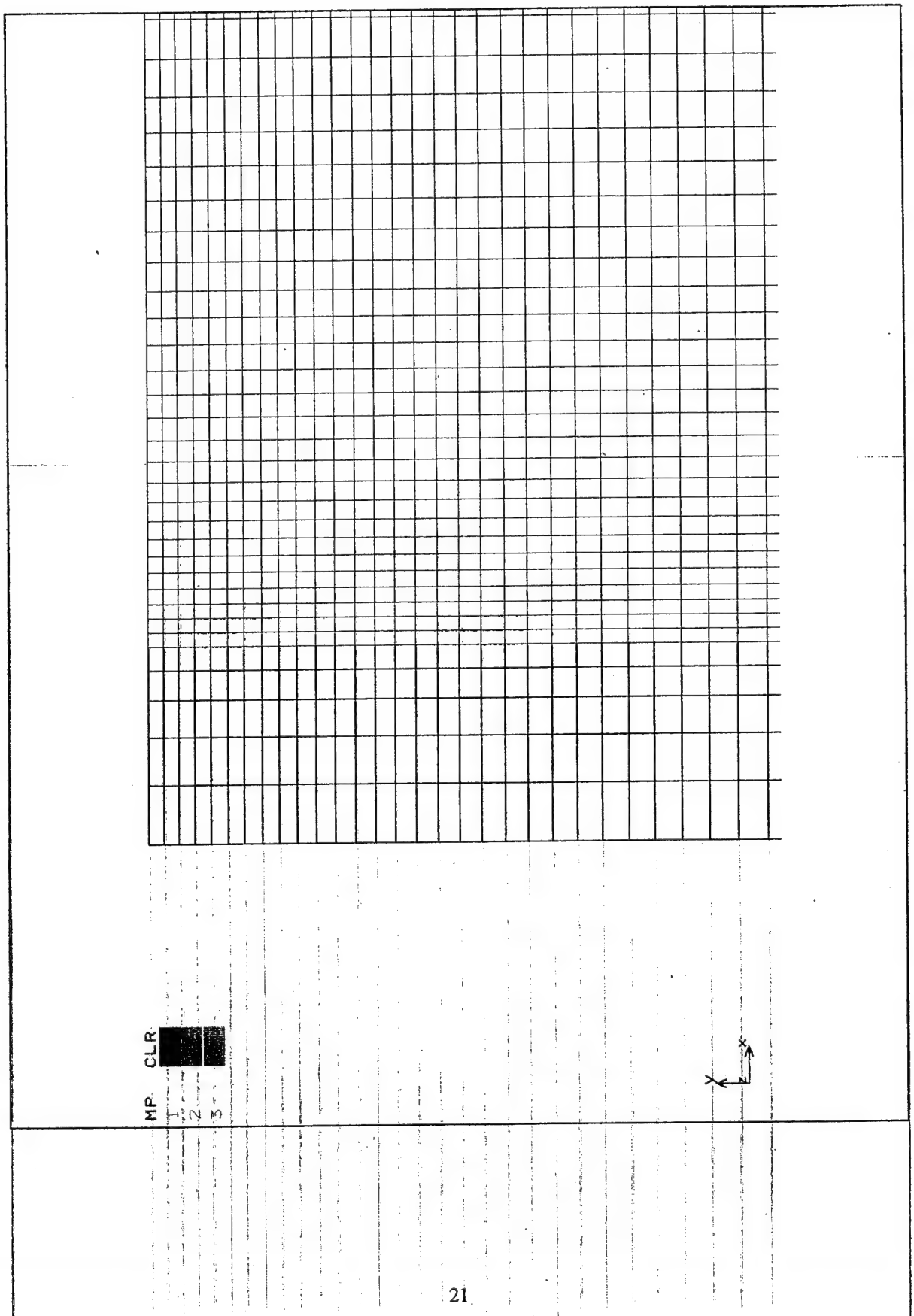

Figure 5 — Enlarged View of Finite Element Mesh

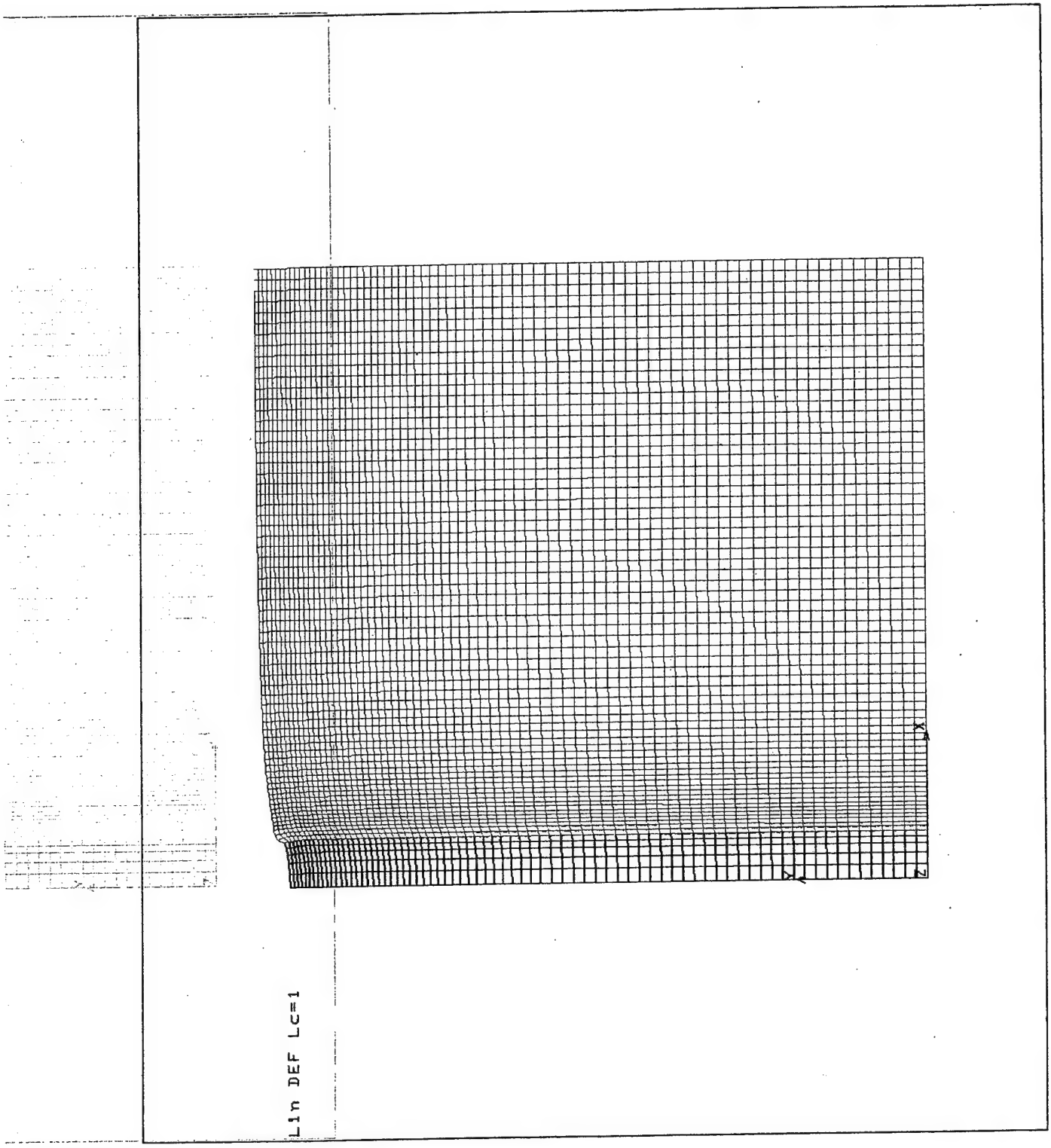

Figure 6 — Thermally Induced Displacements

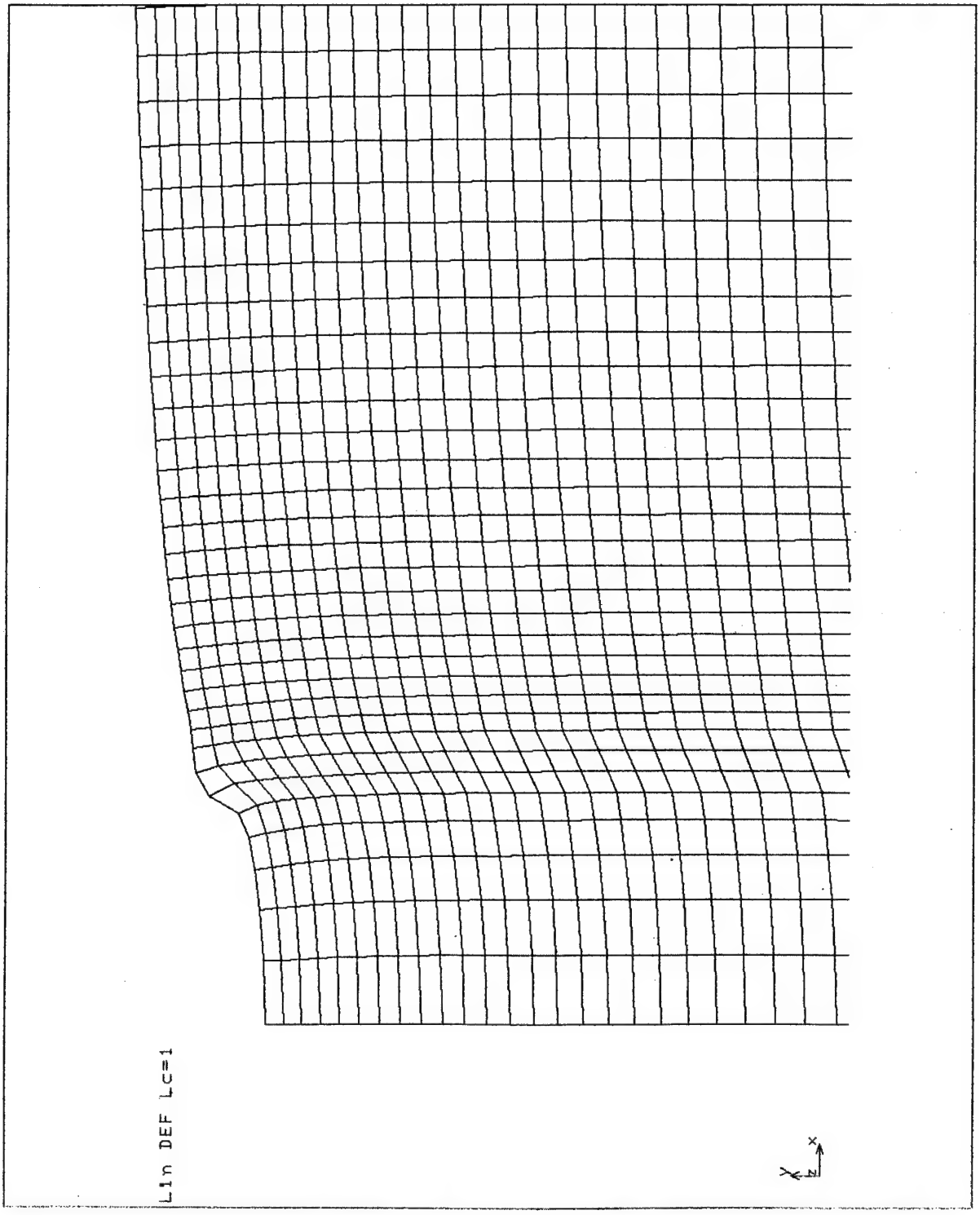

Figure 7 — Enlarged View of Thermally Induced Displacements

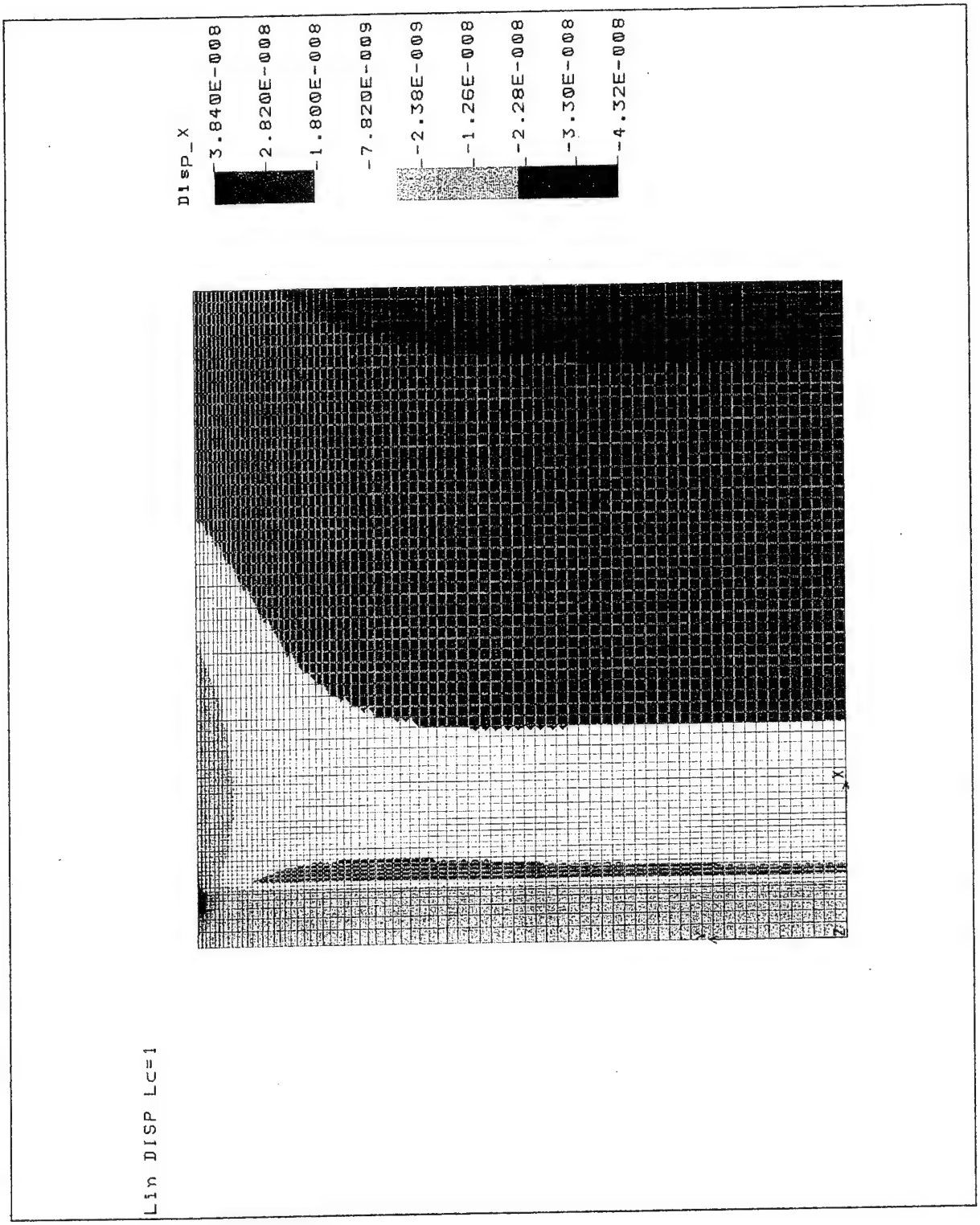

Figure 8 — Radial Displacements (M)

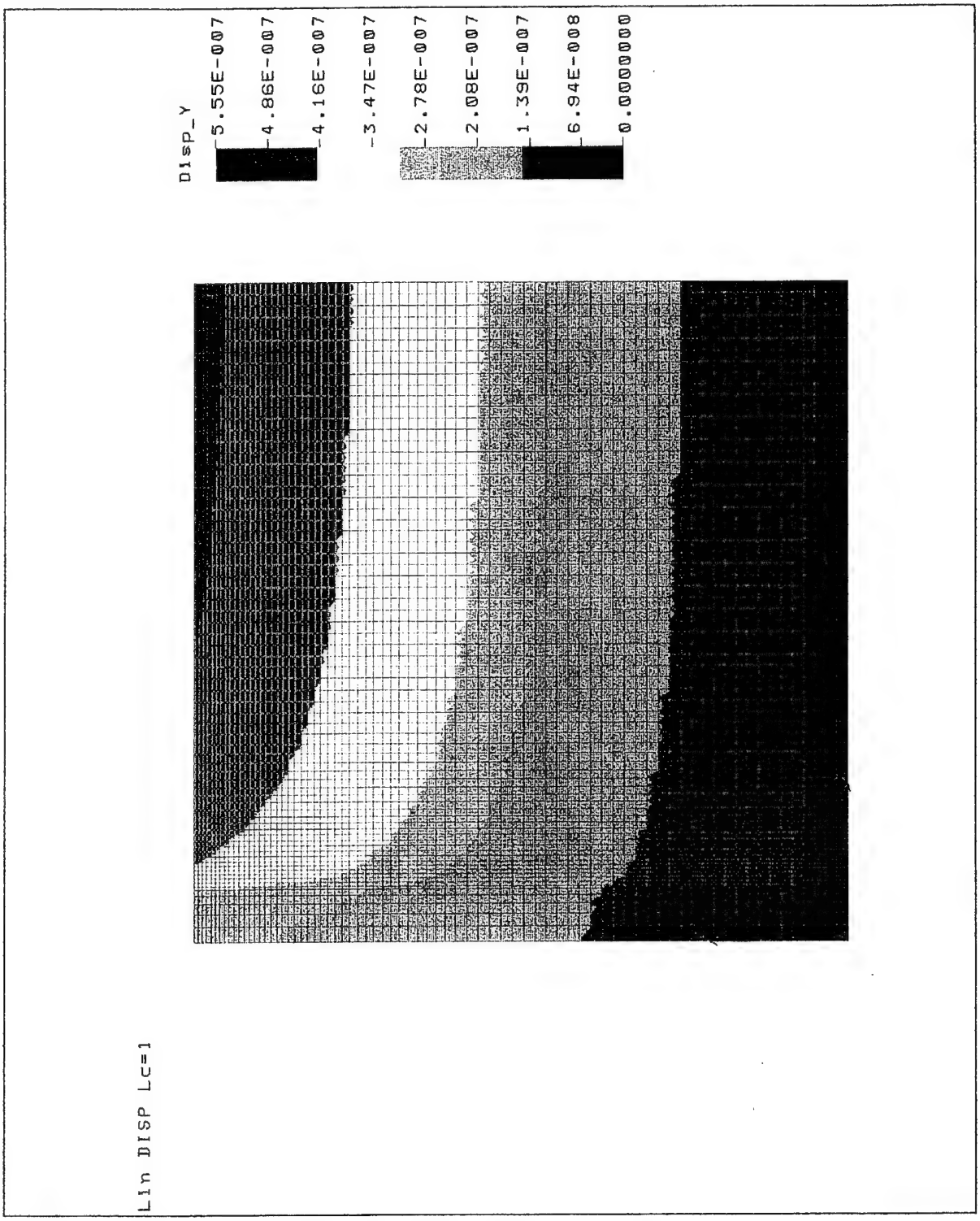

Figure 9 — Axial Displacements (M)

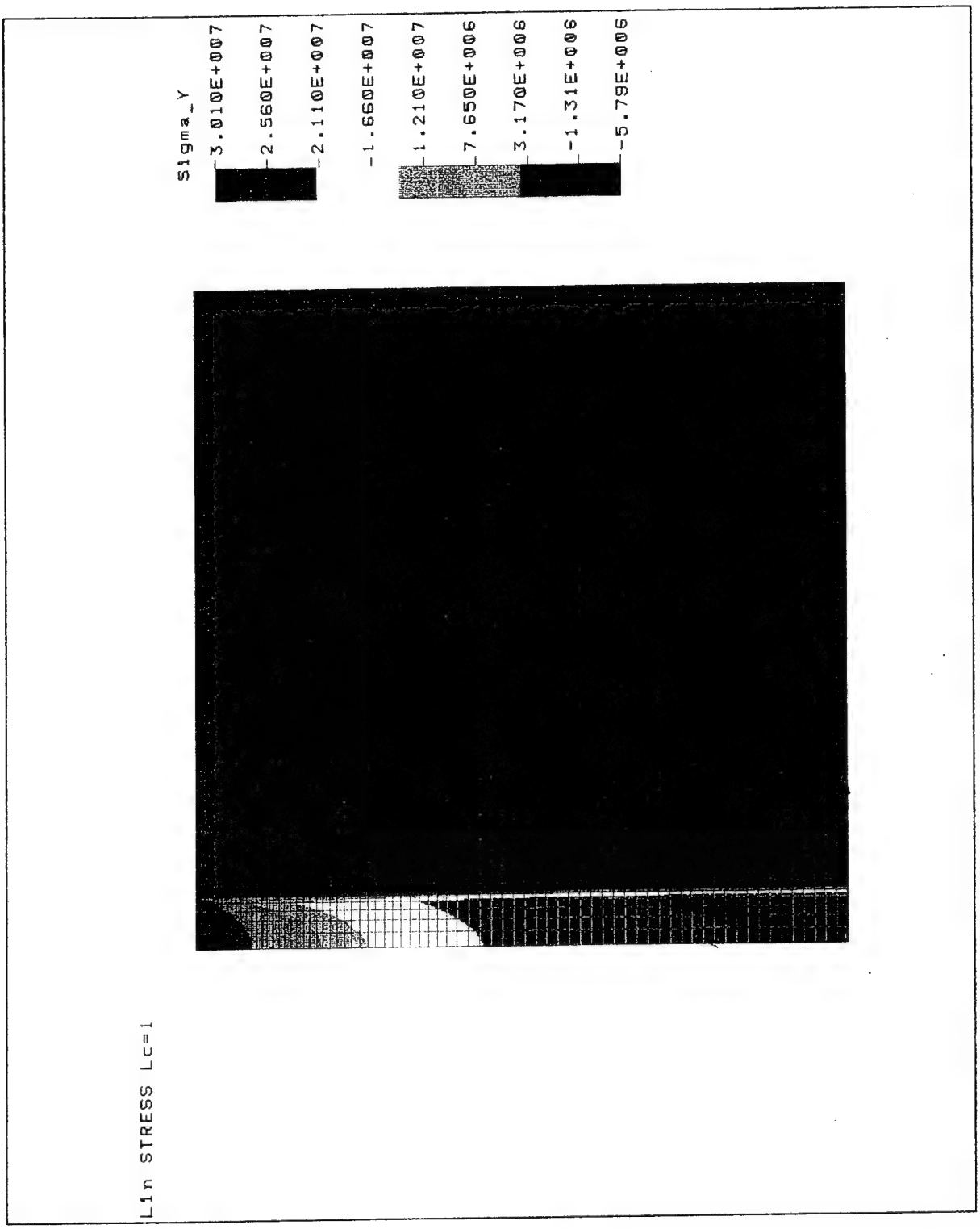

Figure 10 — Through-the-Thickness Normal Stress Field (Pa), Thermal Loads

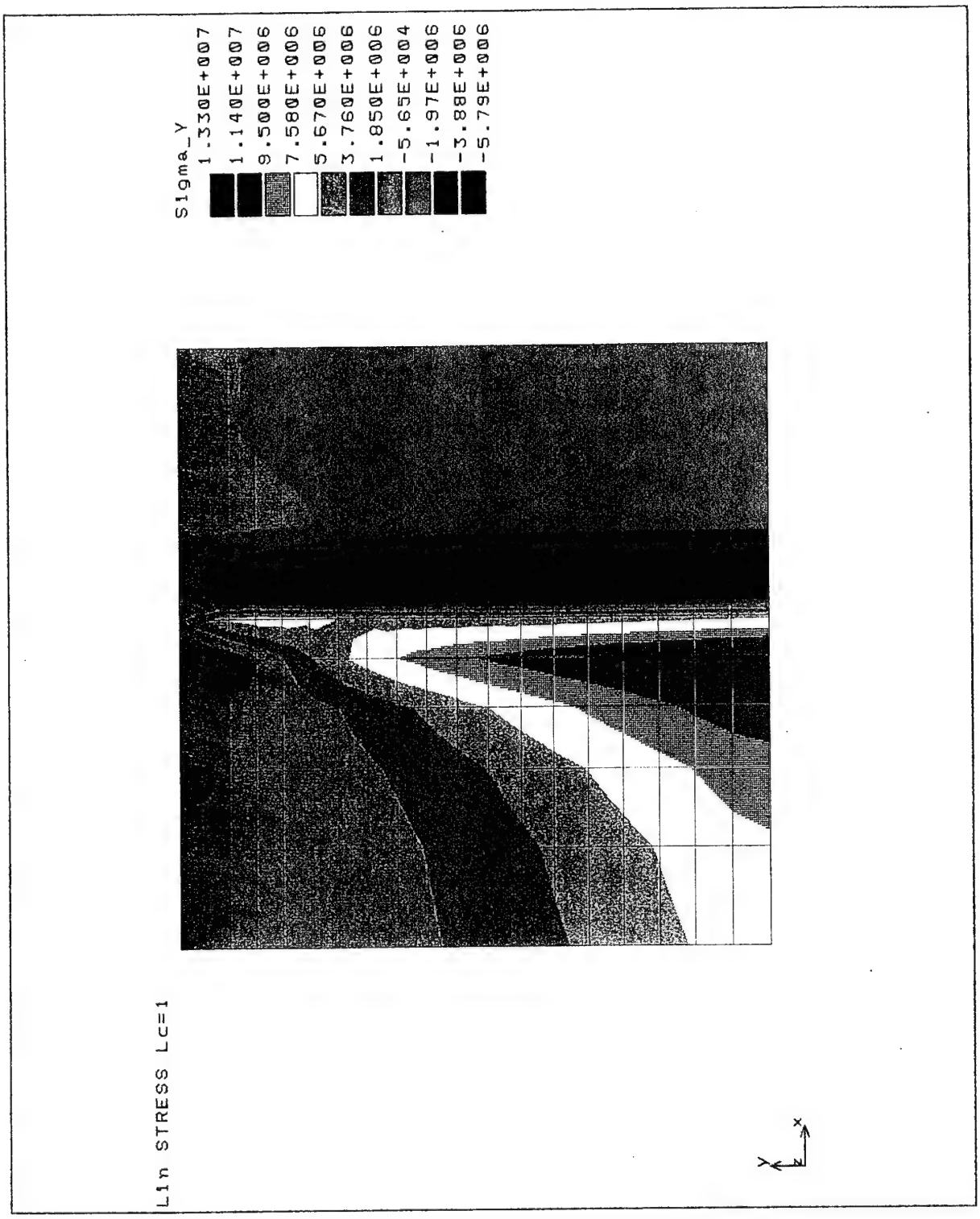

Figure 11 — Enlarged View of the Through-the-Thickness Normal Stress Field (Pa)

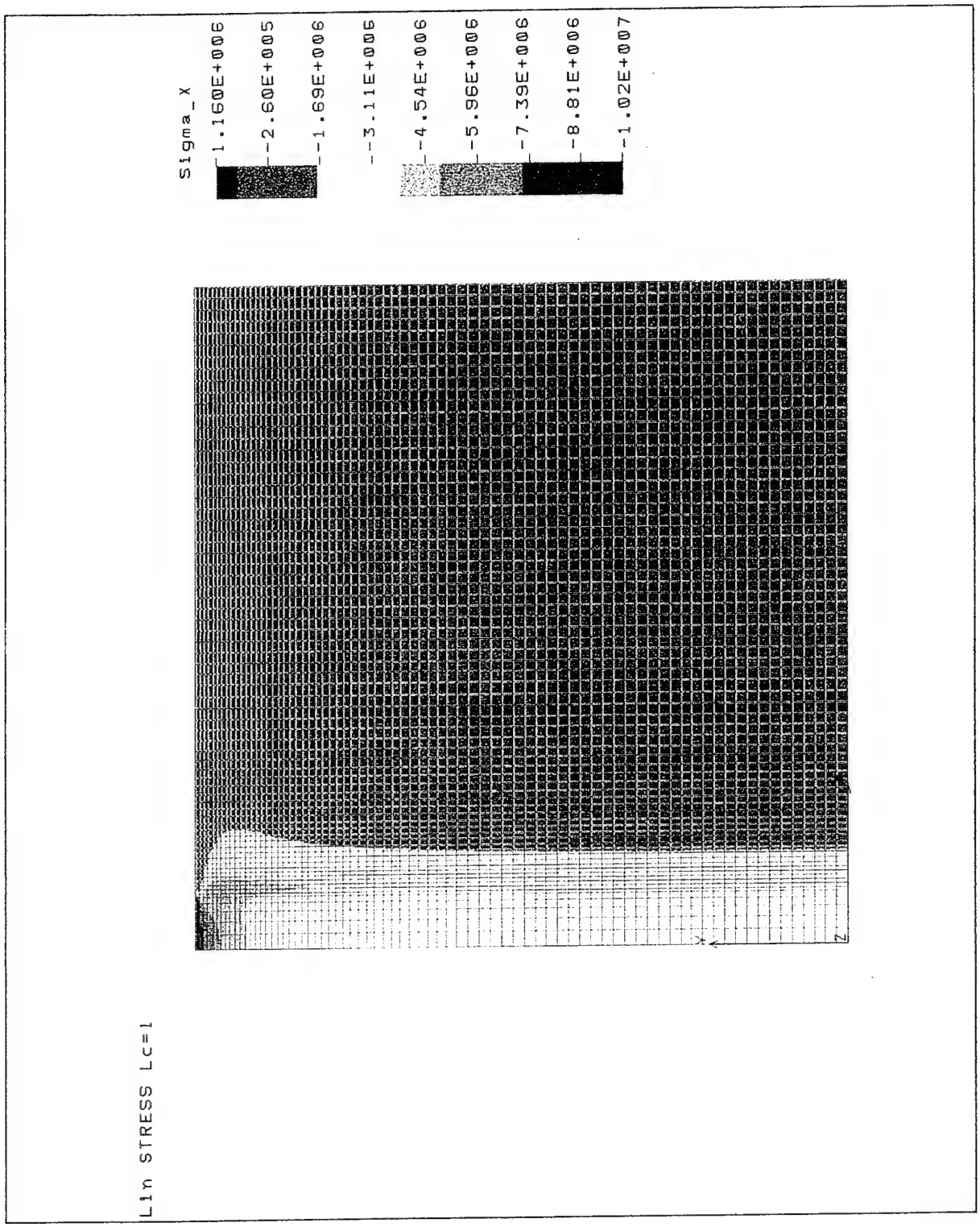

Figure 12 — Radial Stress Field (Pa), Thermal Loads

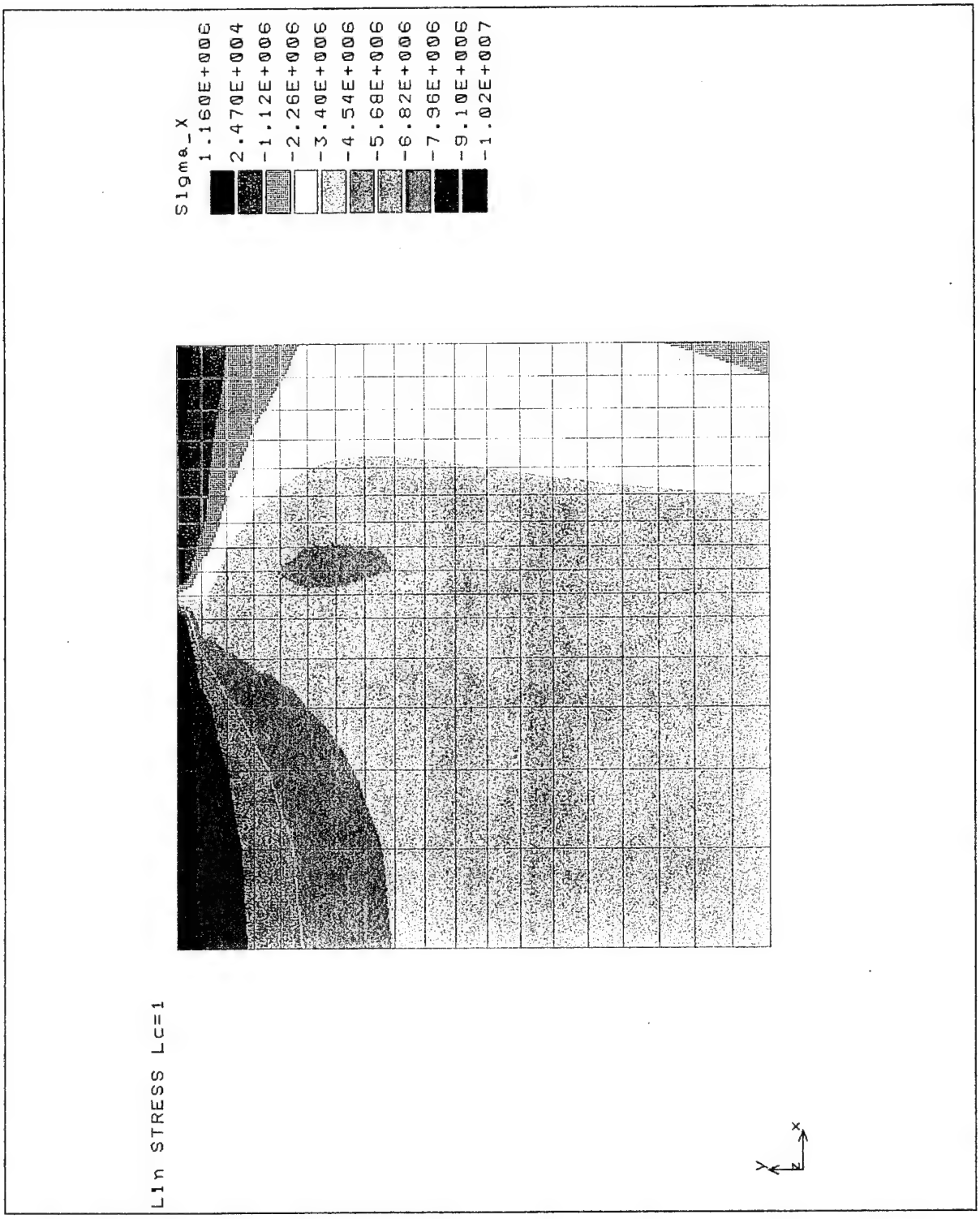

Figure 13 — Enlarged View of the Radial Stress Field (Pa), Thermal Loads

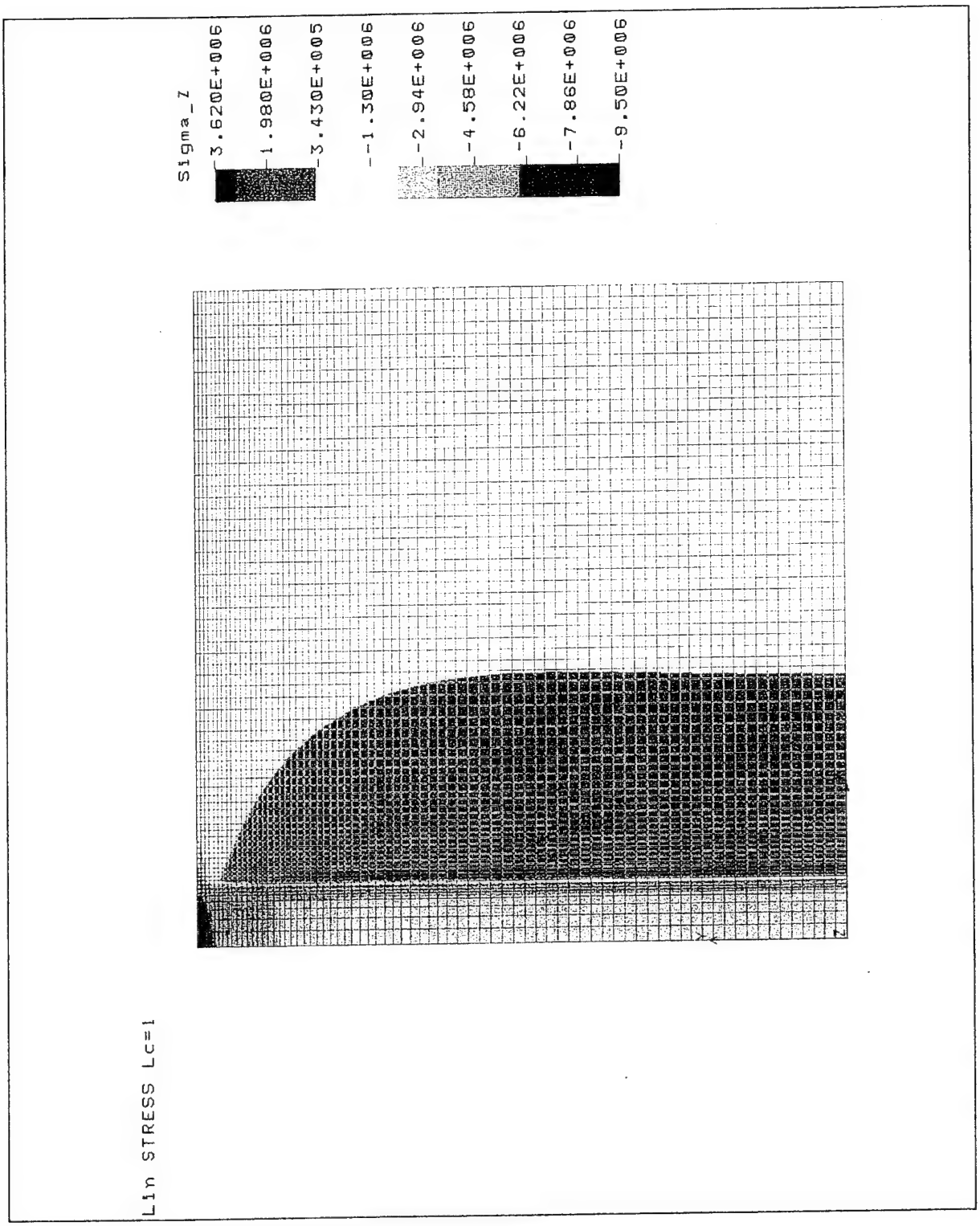

Figure 14 — Hoop Stress Field, (Pa), Thermal Loads

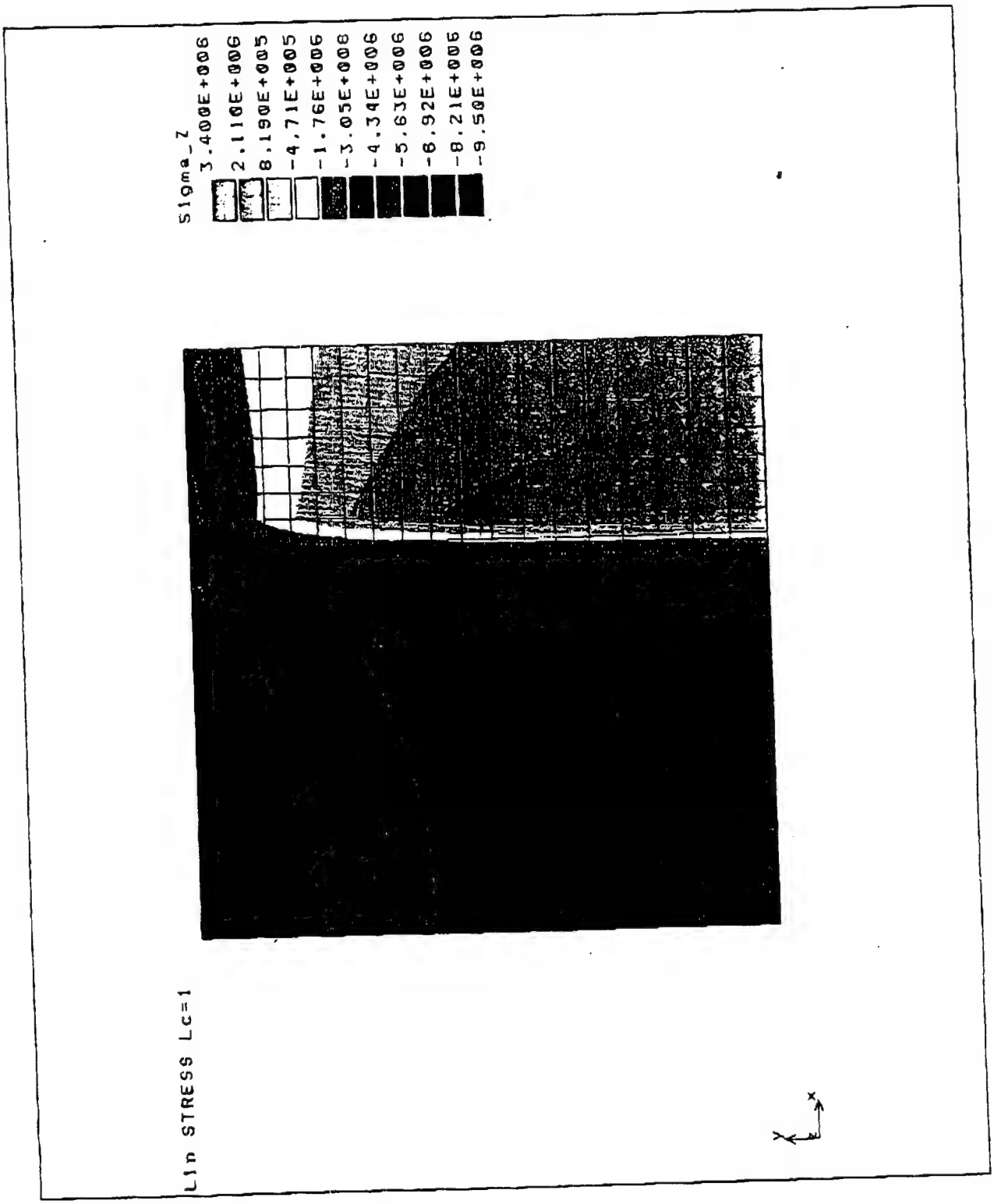

Figure 15 — Enlarged View of the Hoop Stress Field (Pa), Thermal Loads

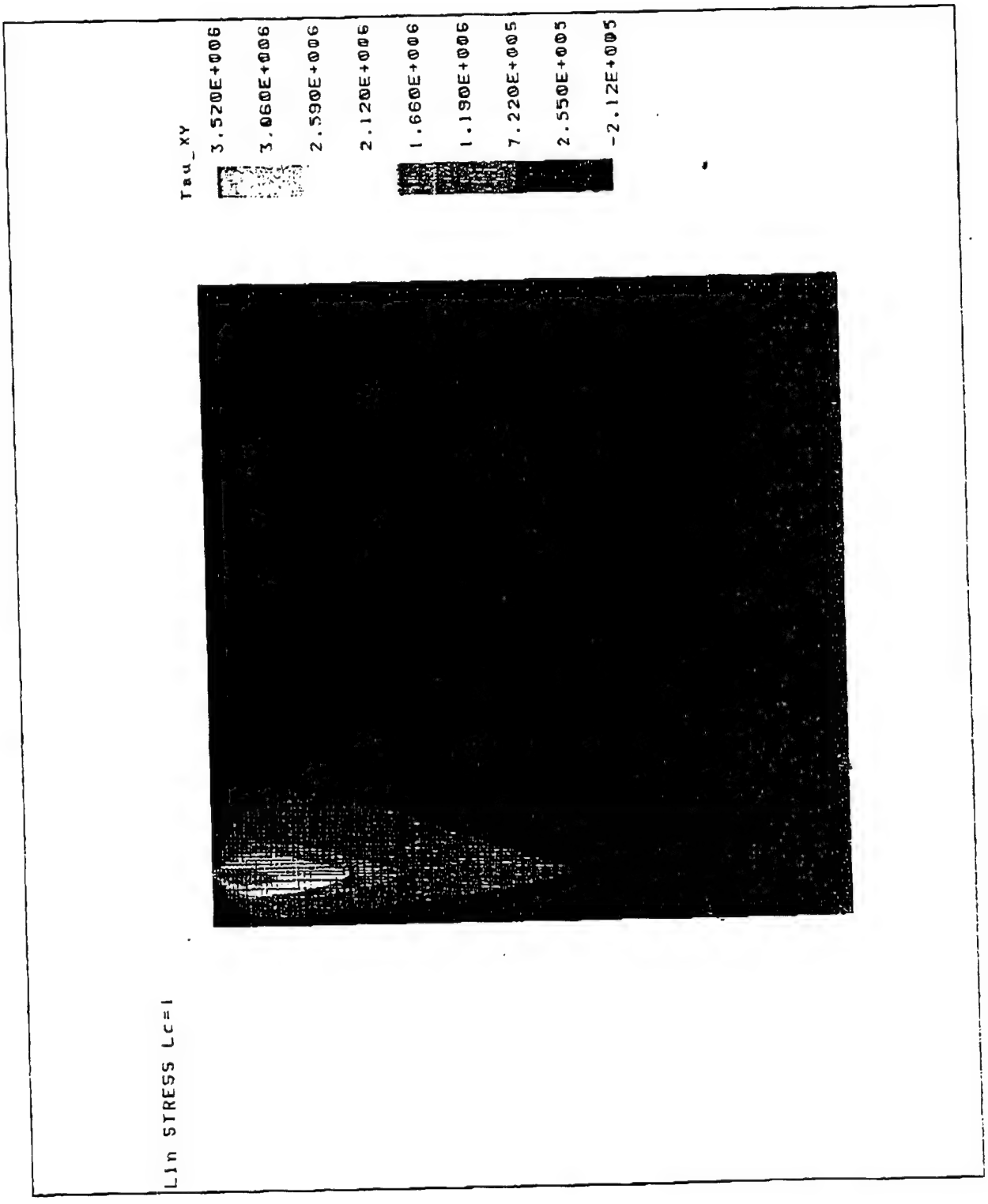

Figure 16 — Shear Stress Field (Pa), Thermal Loads

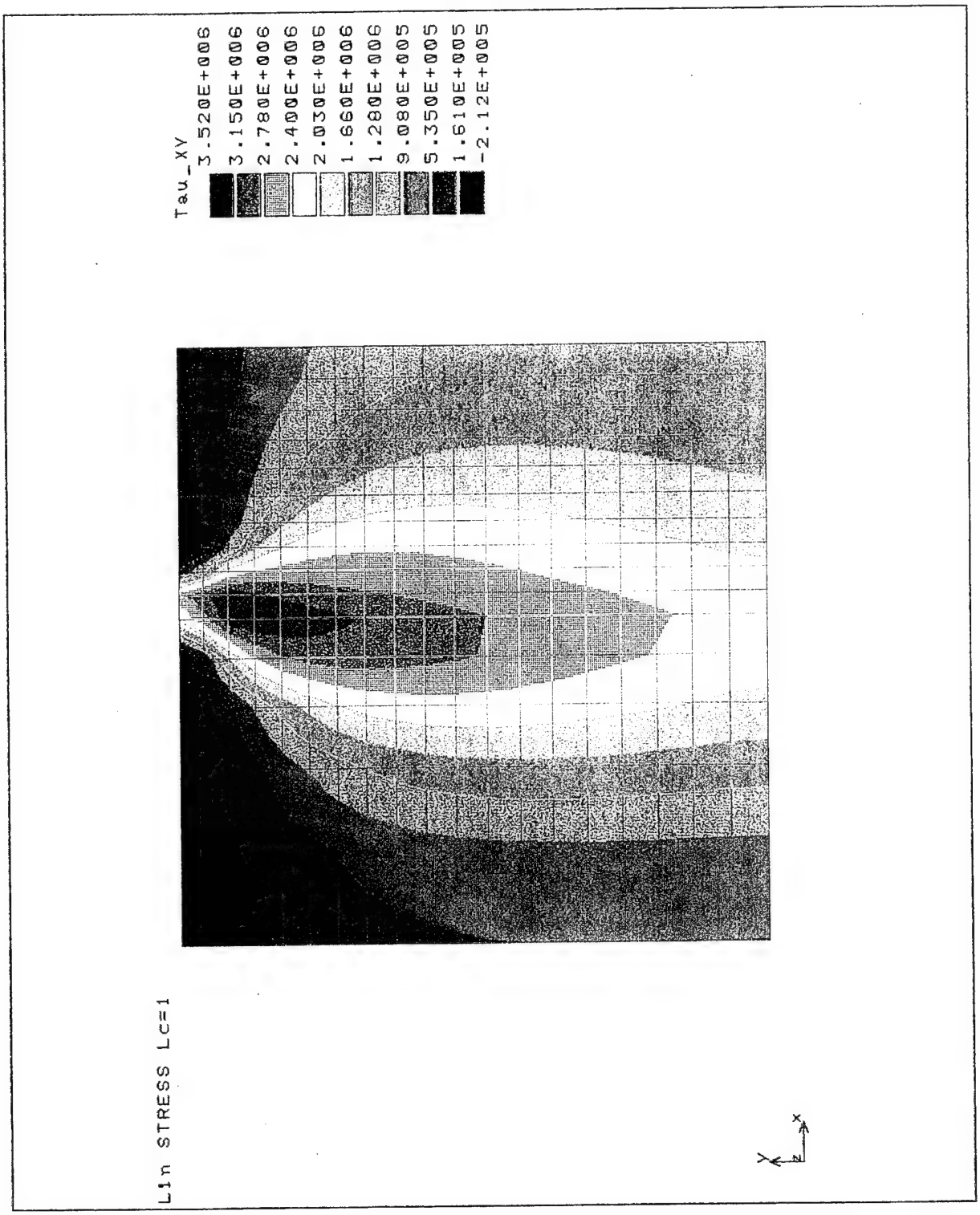

Figure 17 — Enlarged View of the Shear Stress Field (Pa), Thermal Loads

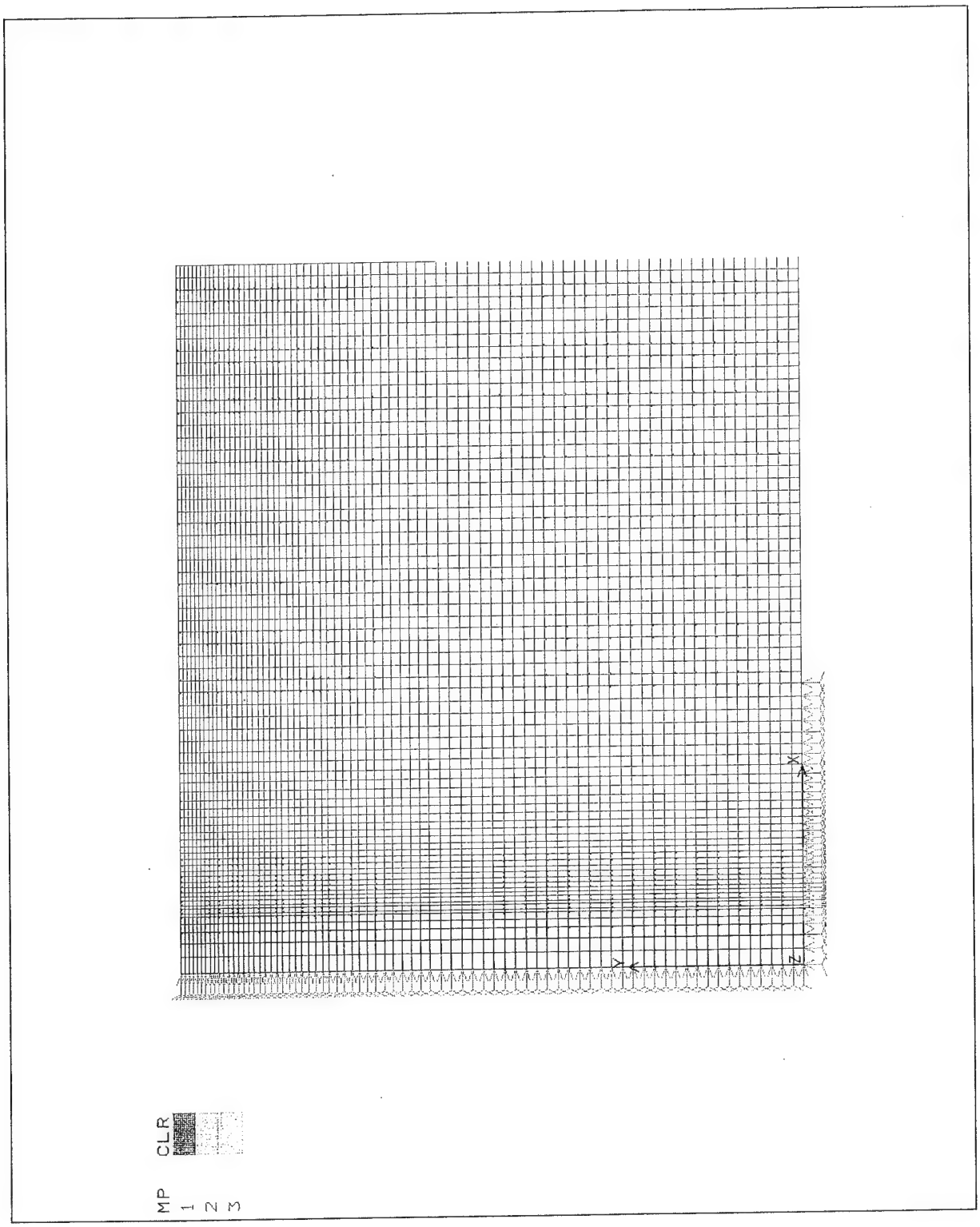

Figure 18 — Finite Element Mesh with Boundary Conditions for Modeling the Crack

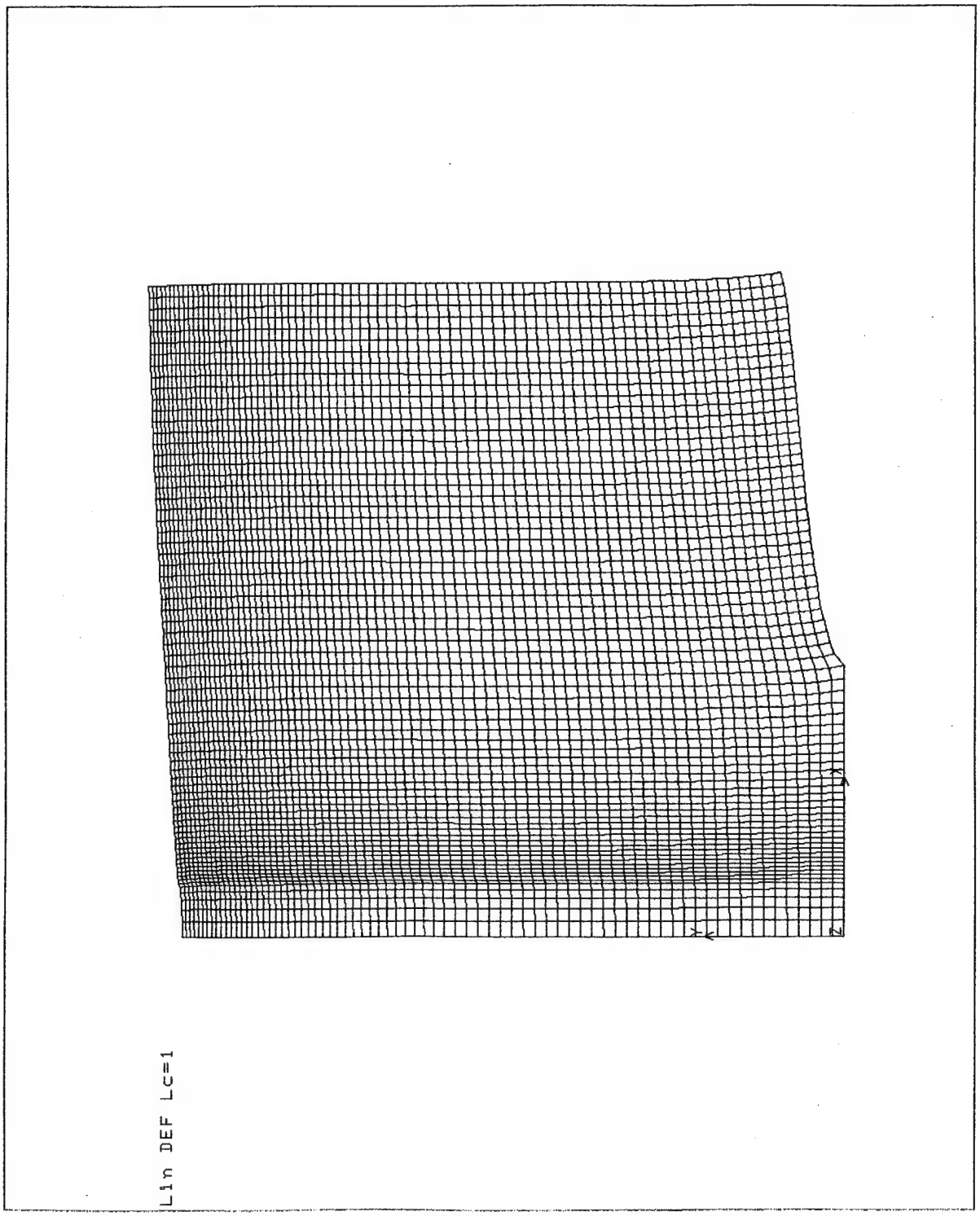

Figure 19 — Displacements due to Crack Opening Loads

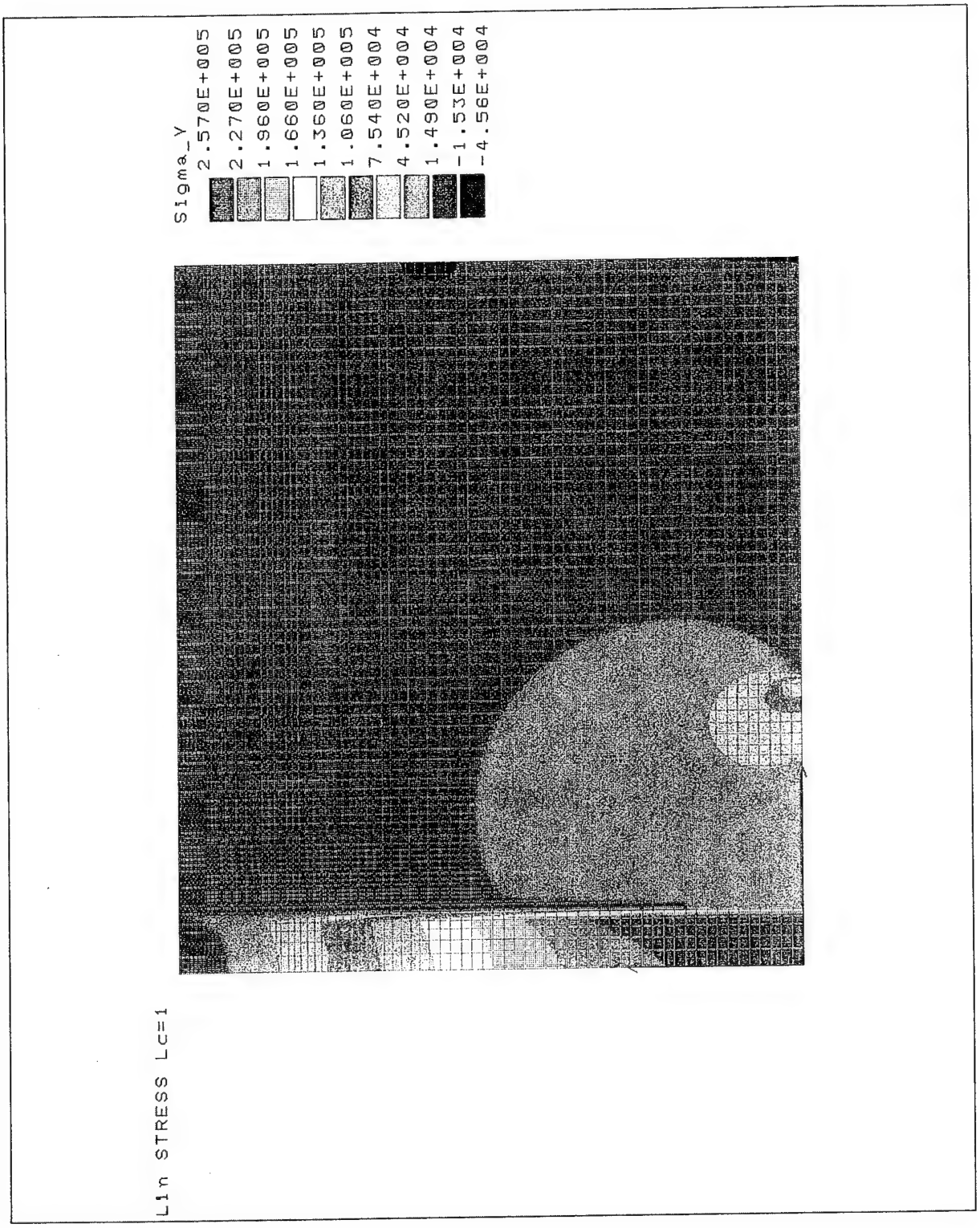

Figure 20 — Through-the-Thickness Normal Stress Field (Pa), Crack Opening Loads

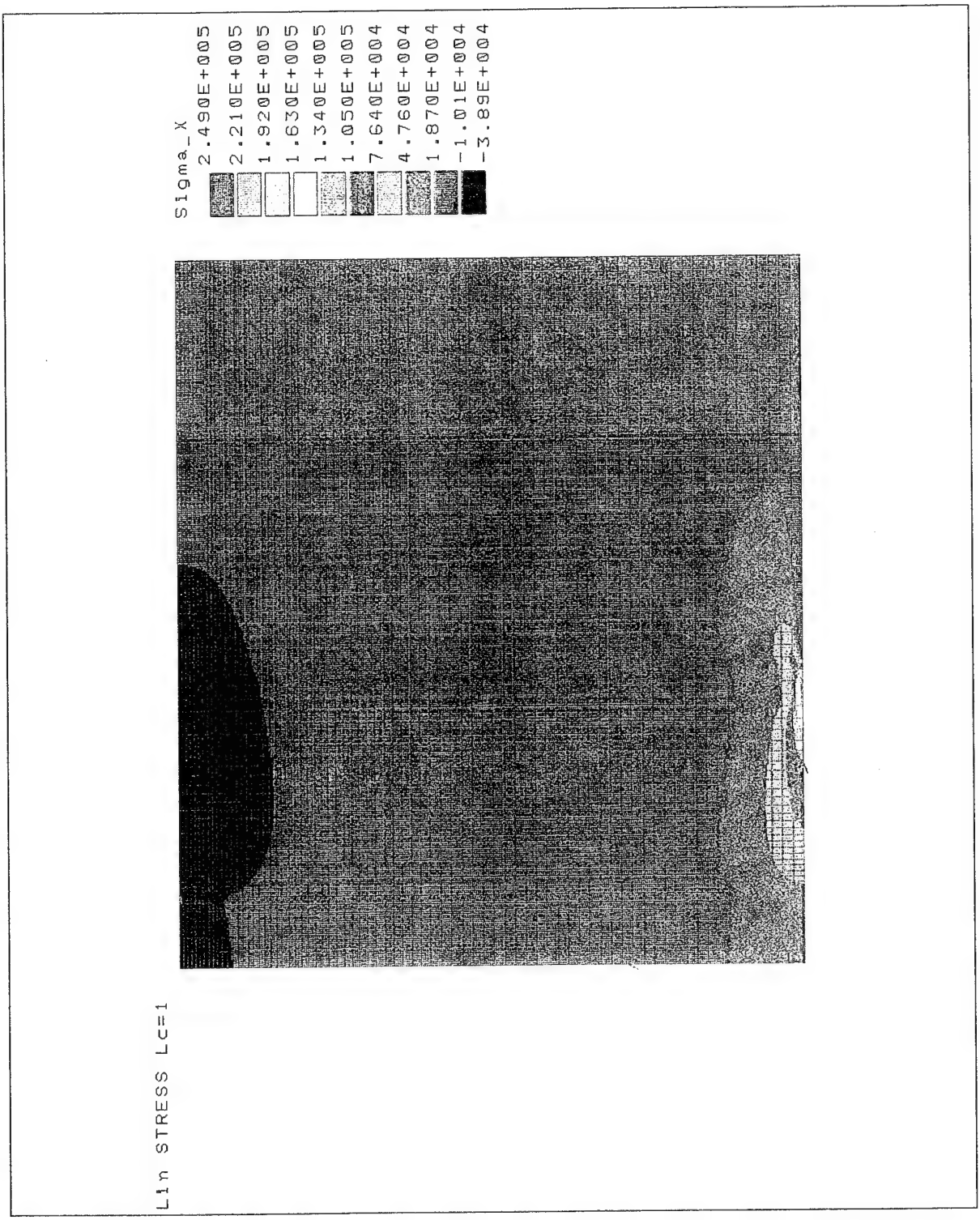

Figure 21 — Radial Stress Field (Pa), Crack Opening Loads

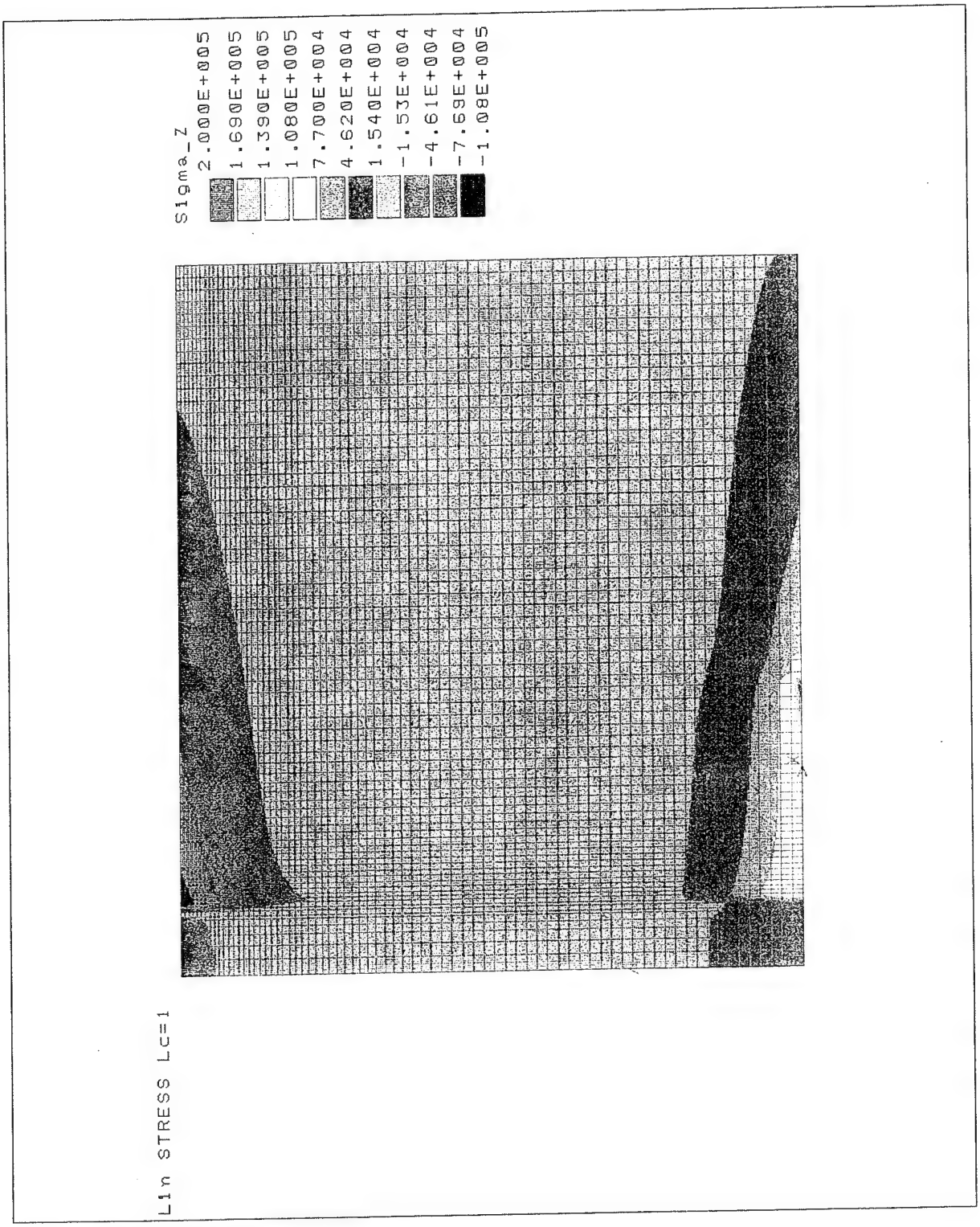

Figure 22 — Hoop Stress Field (Pa), Crack Opening Loads

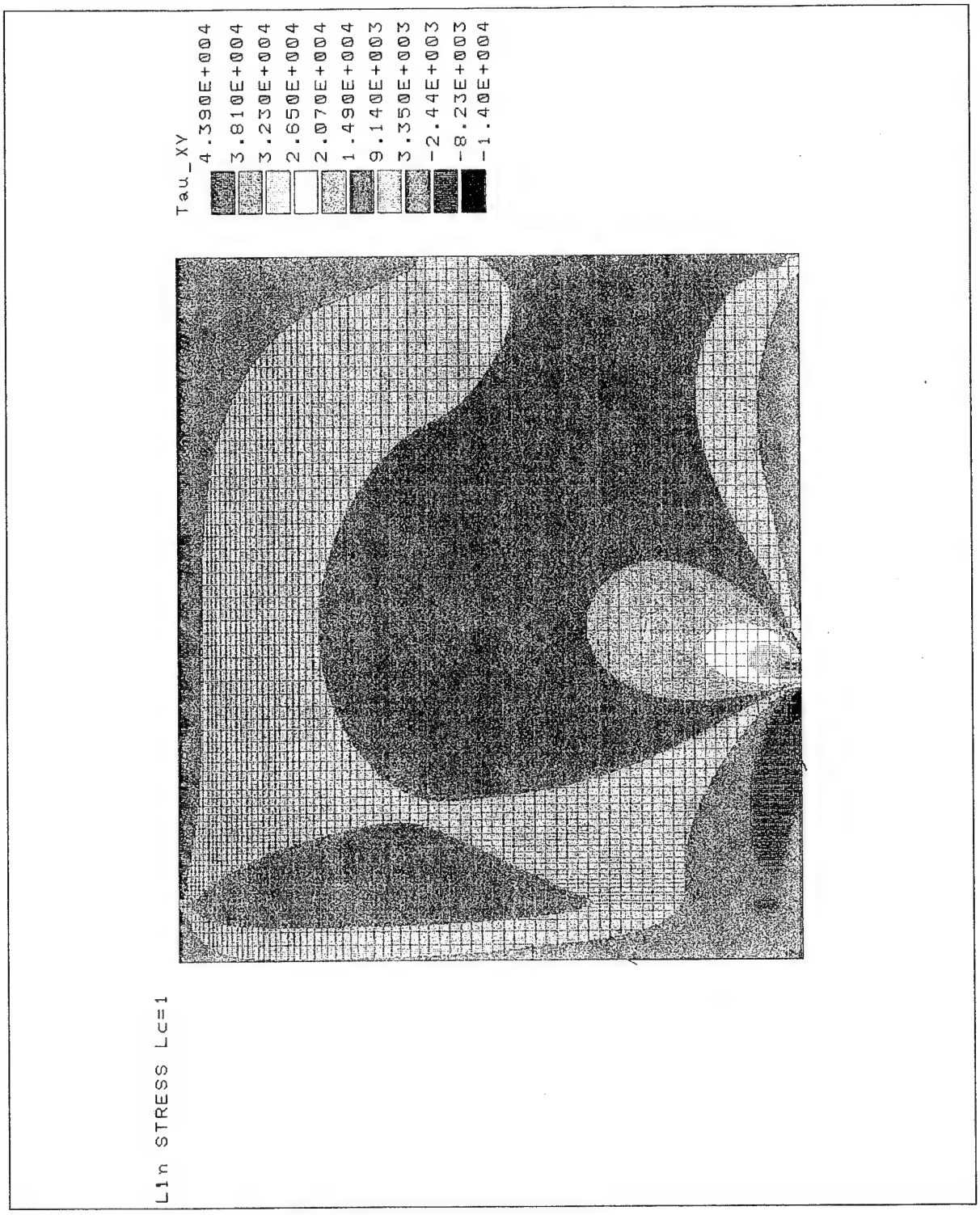

Figure 23 — Shear Stress Field (Pa), Crack Opening Loads

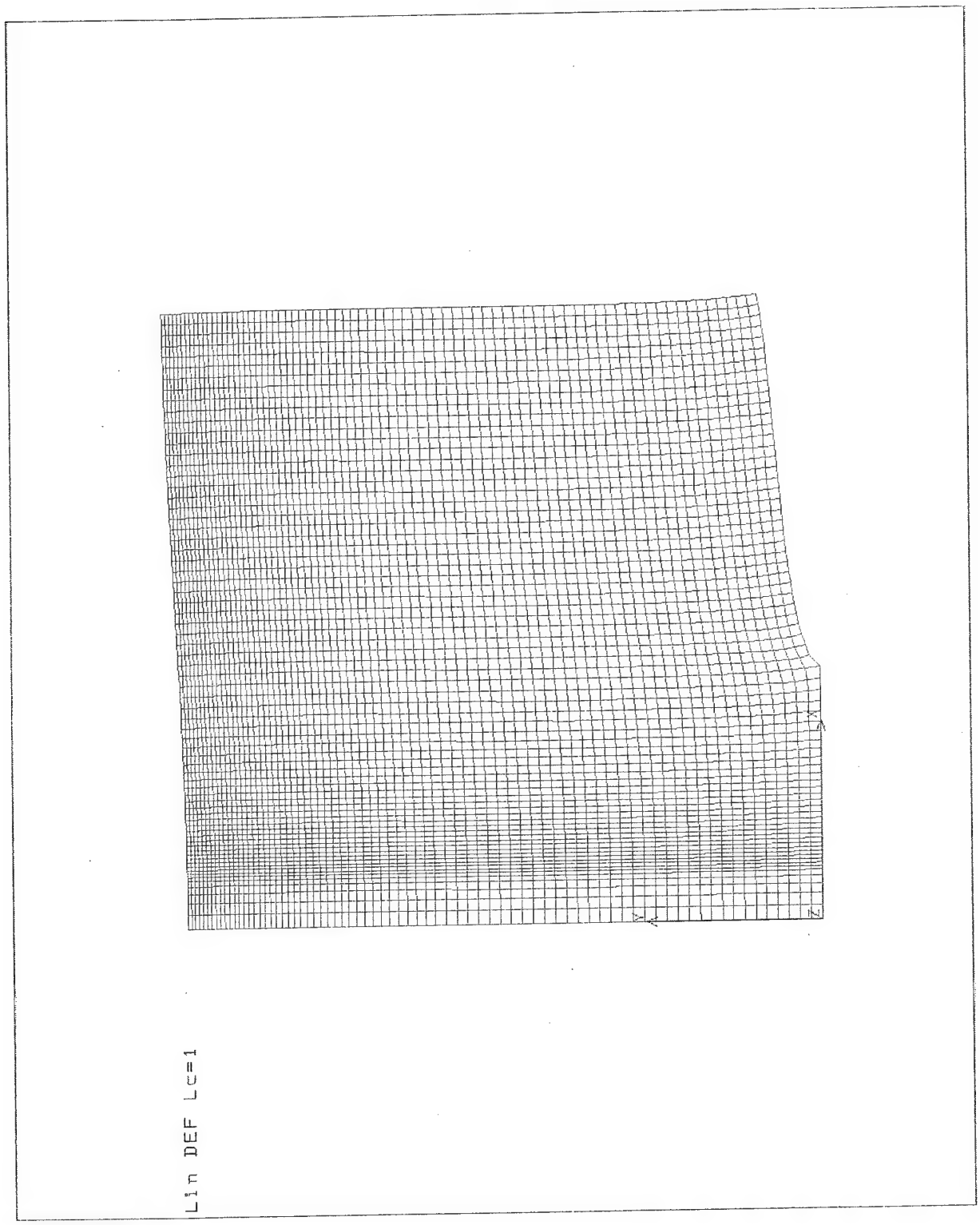

Figure 24 — Displacements in the Unreinforced Case

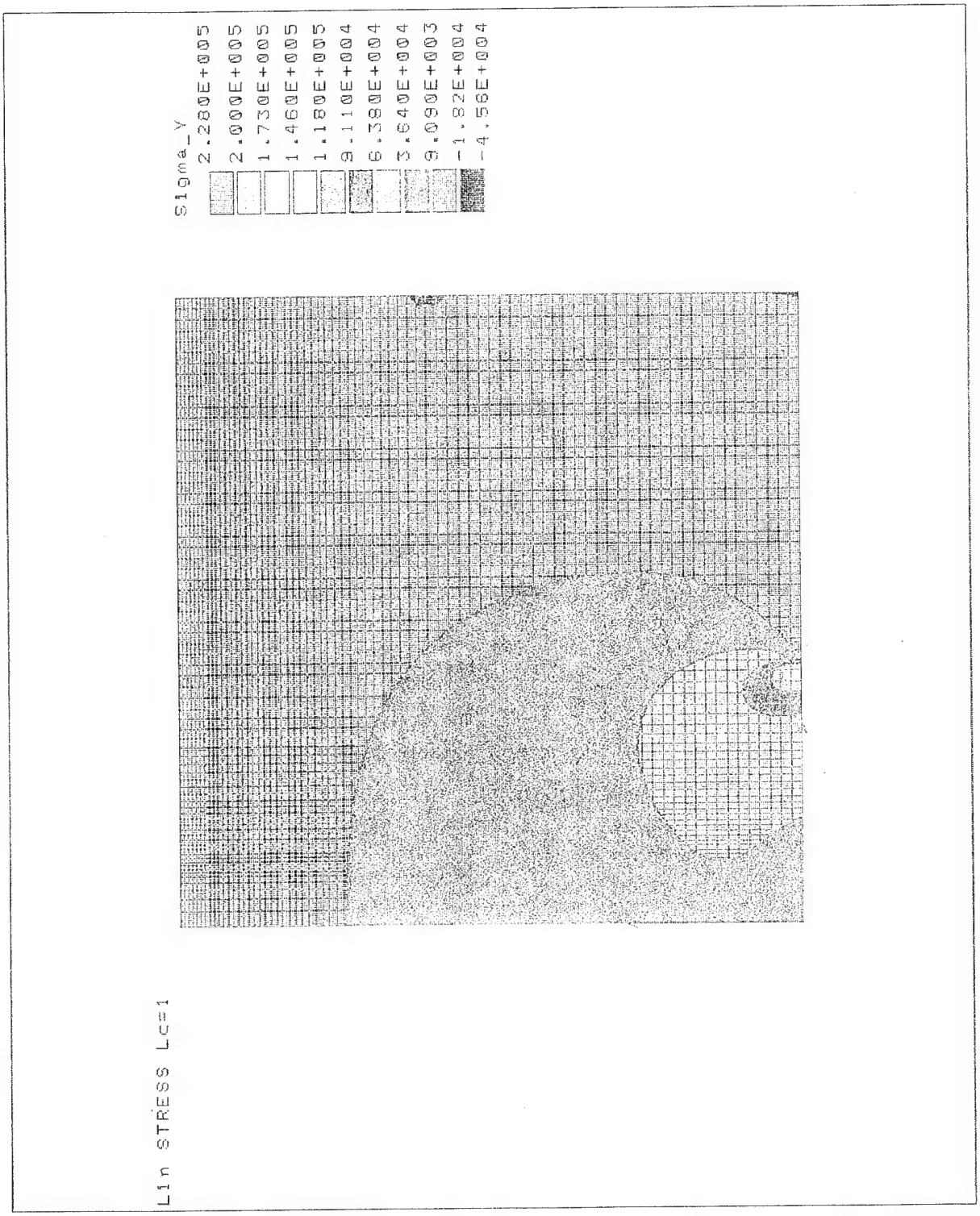

Figure 25 — Through-the-Thickness Normal Stress Field (Pa), Unreinforced Case

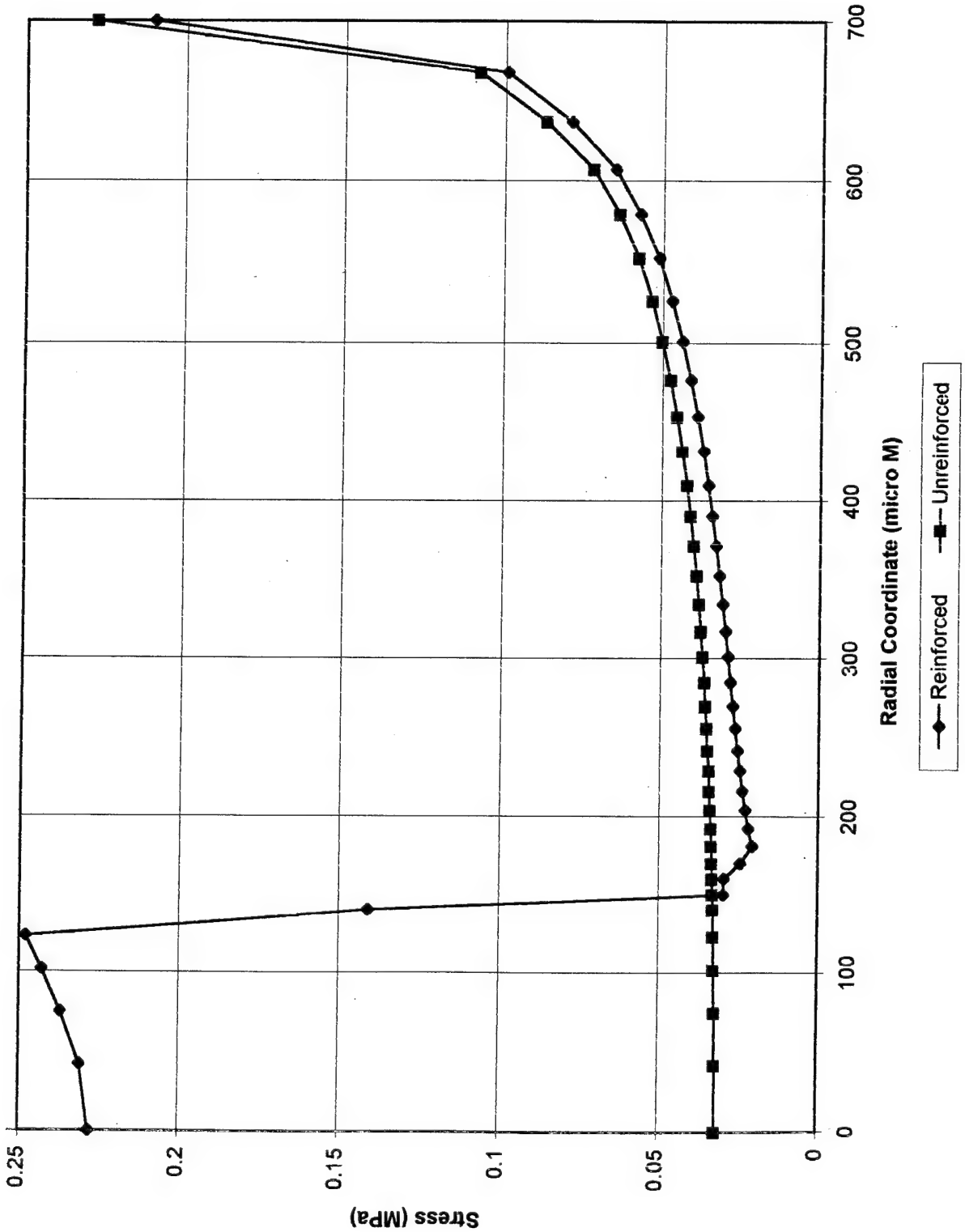

Figure 26 — Through-the-Thickness Normal Stresses at the Mid-Plane

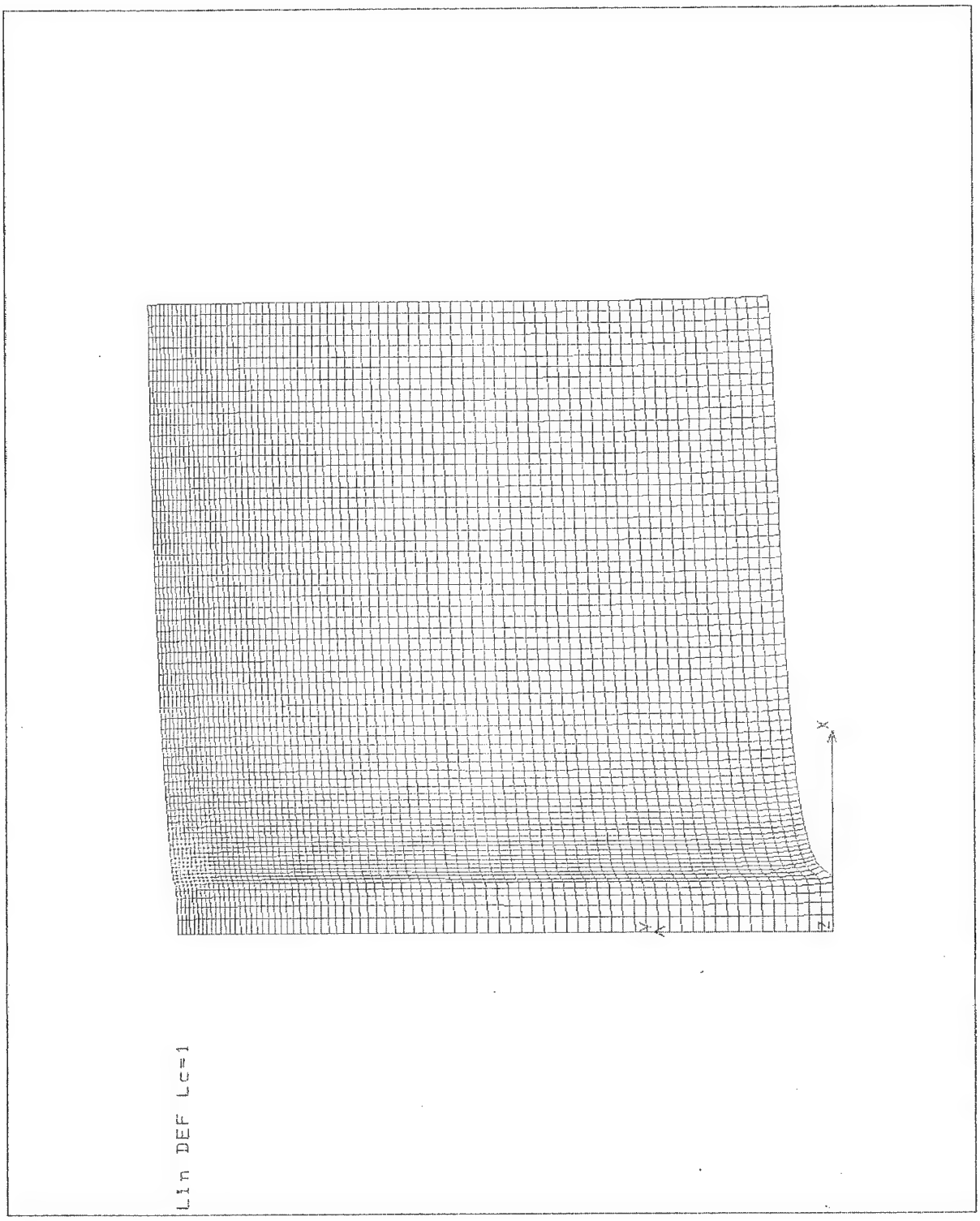

Figure 27 — Displacements due to Crack Opening Loads, Crack to Fiber

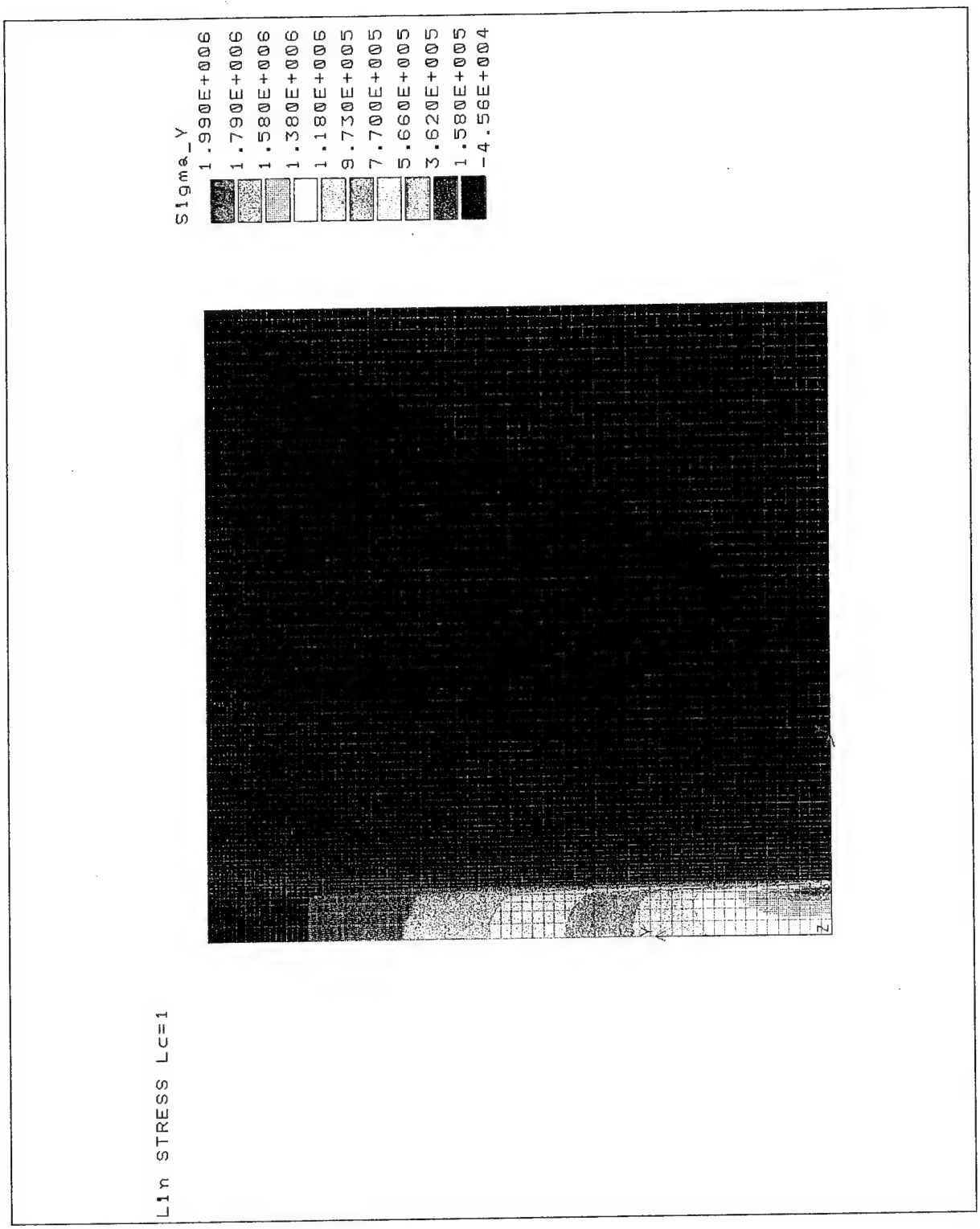

Figure 28 — Through-the-Thickness Normal Stress Field (Pa), Crack Opening Loads

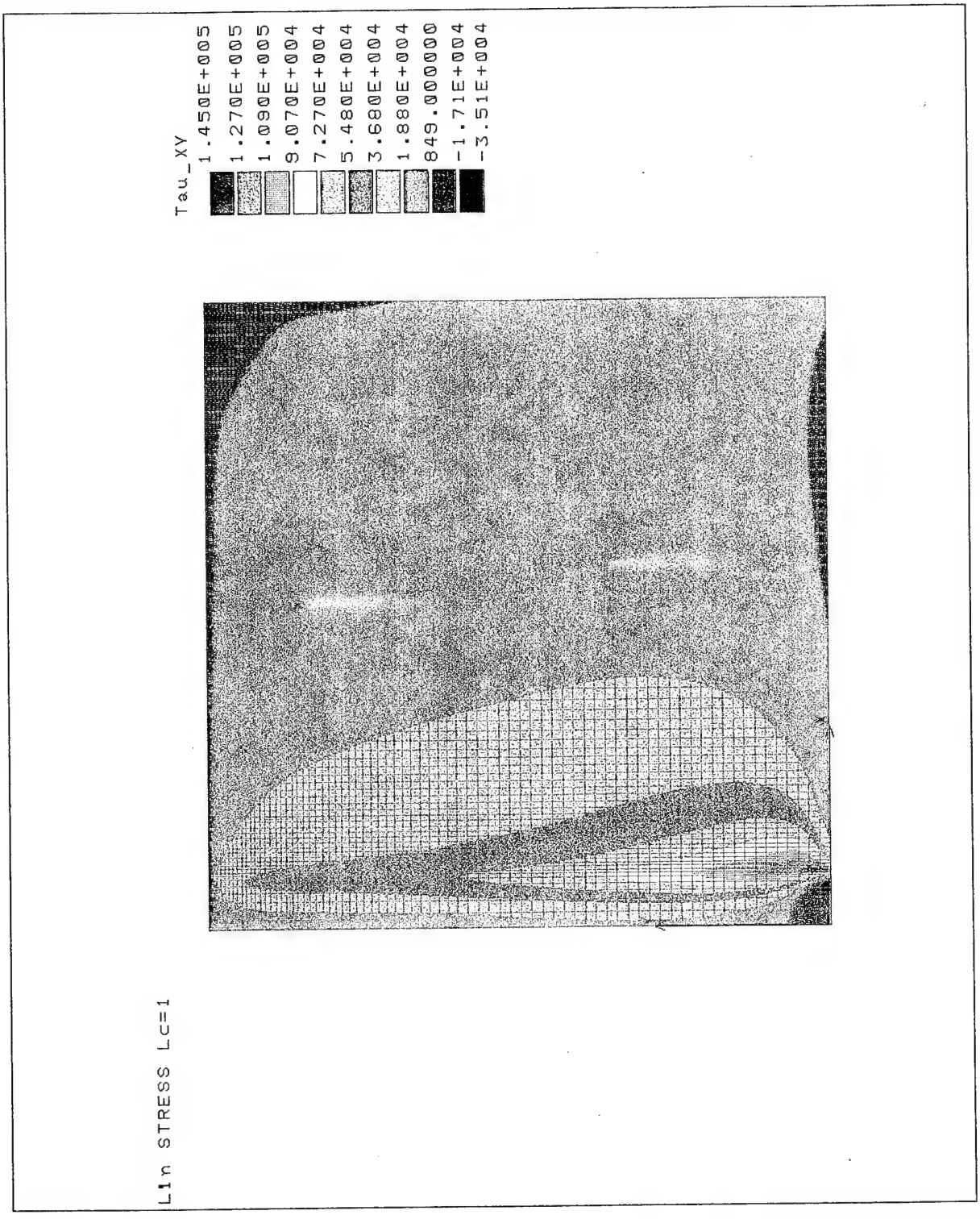

Figure 29 — Shear Stress Field (Pa), Crack Opening Loads

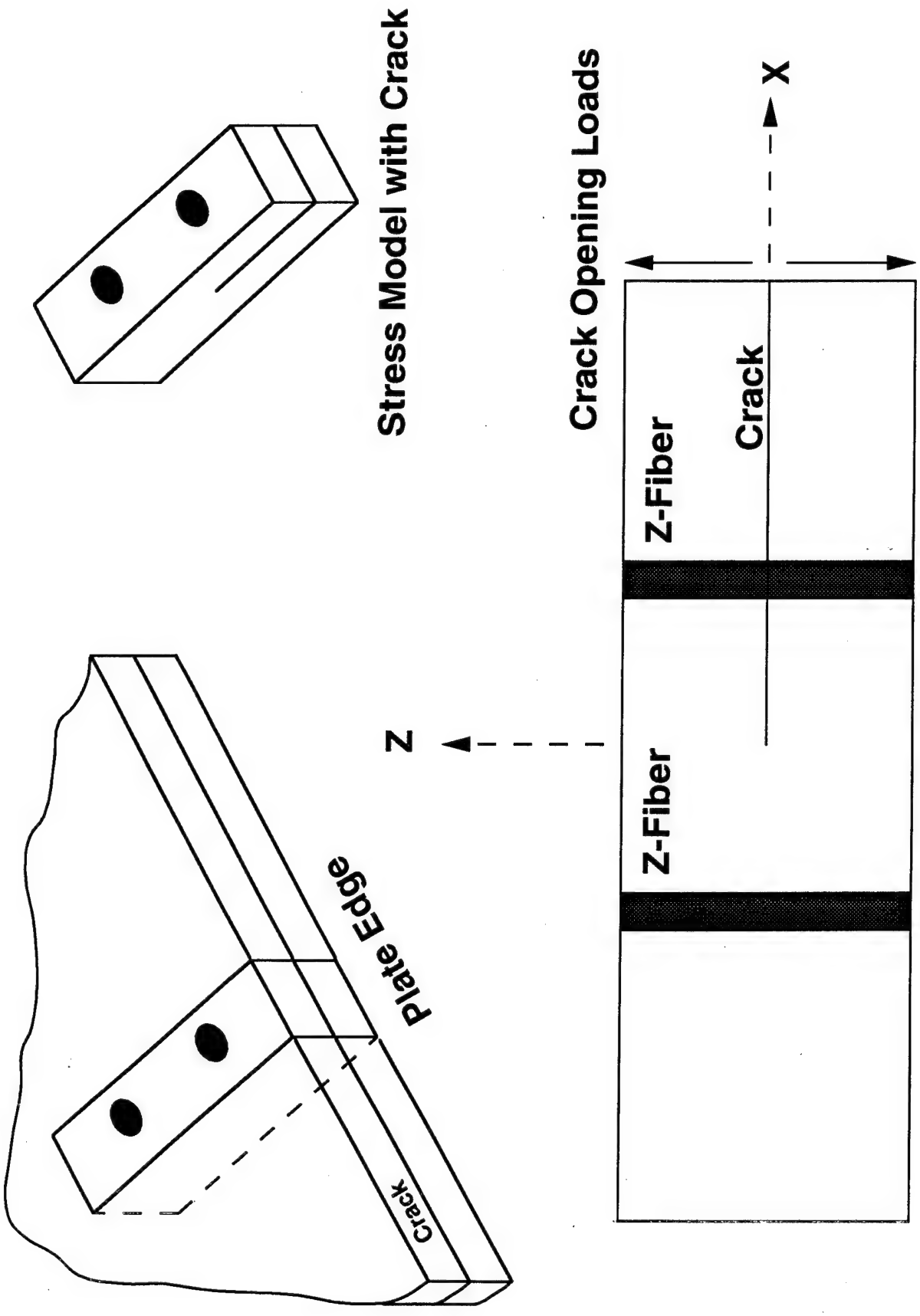

Figure 30 — Mode I Loads and Edge Crack (Not to Scale)

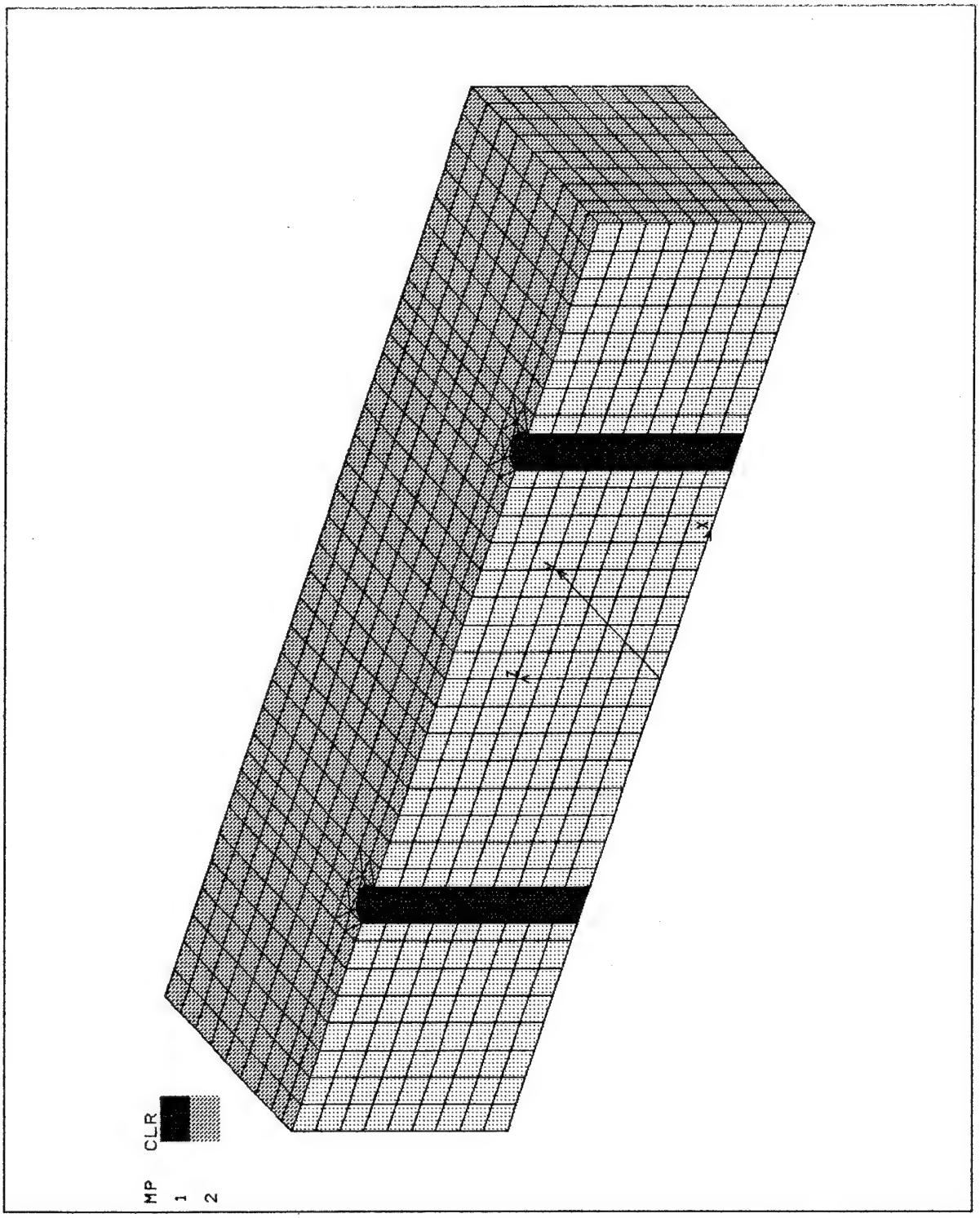

Figure 31 — Three-Dimensional Finite Element Mesh

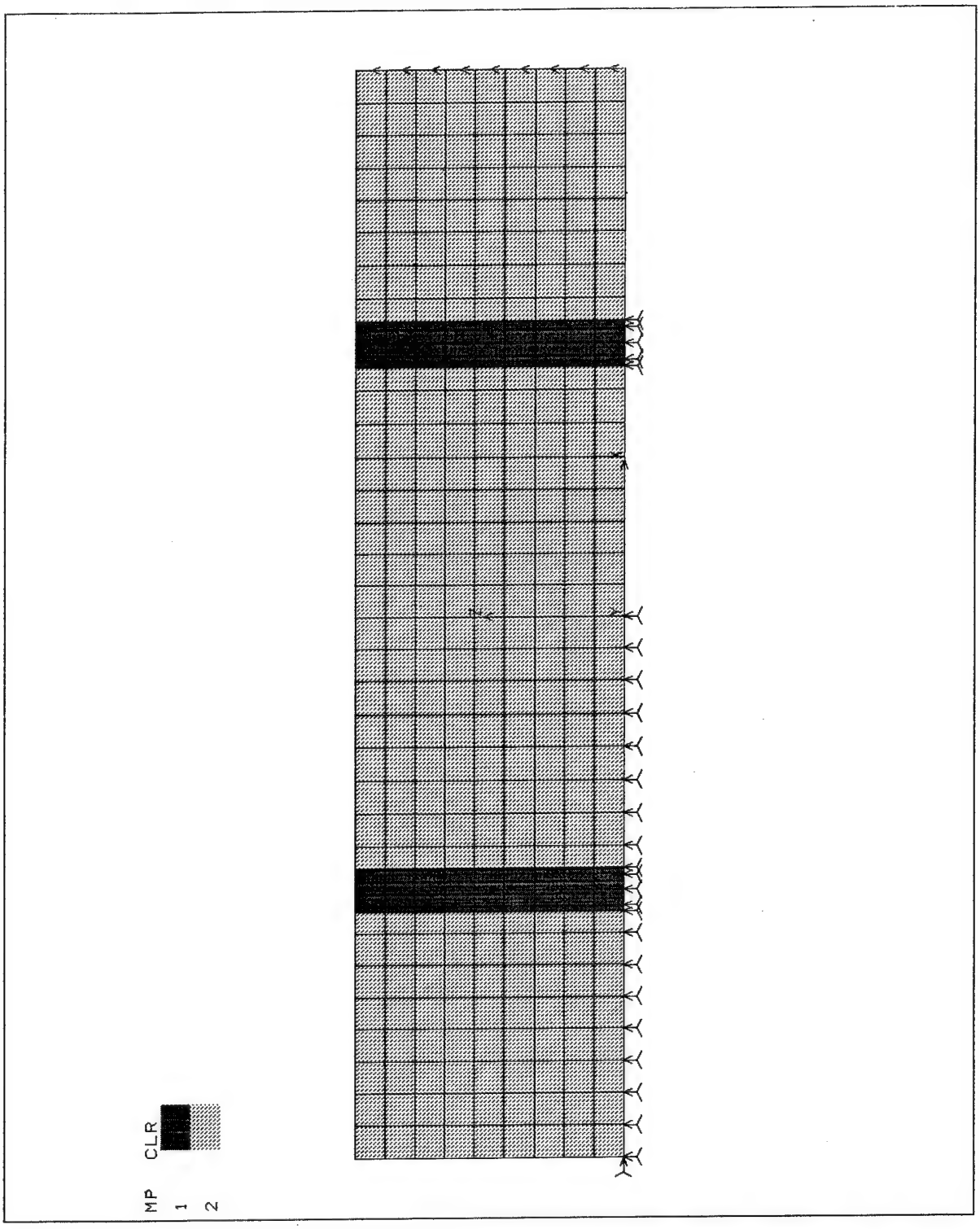

Figure 32 — Boundary Conditions as Viewed from the Negative Y-Axis, Pin Intact

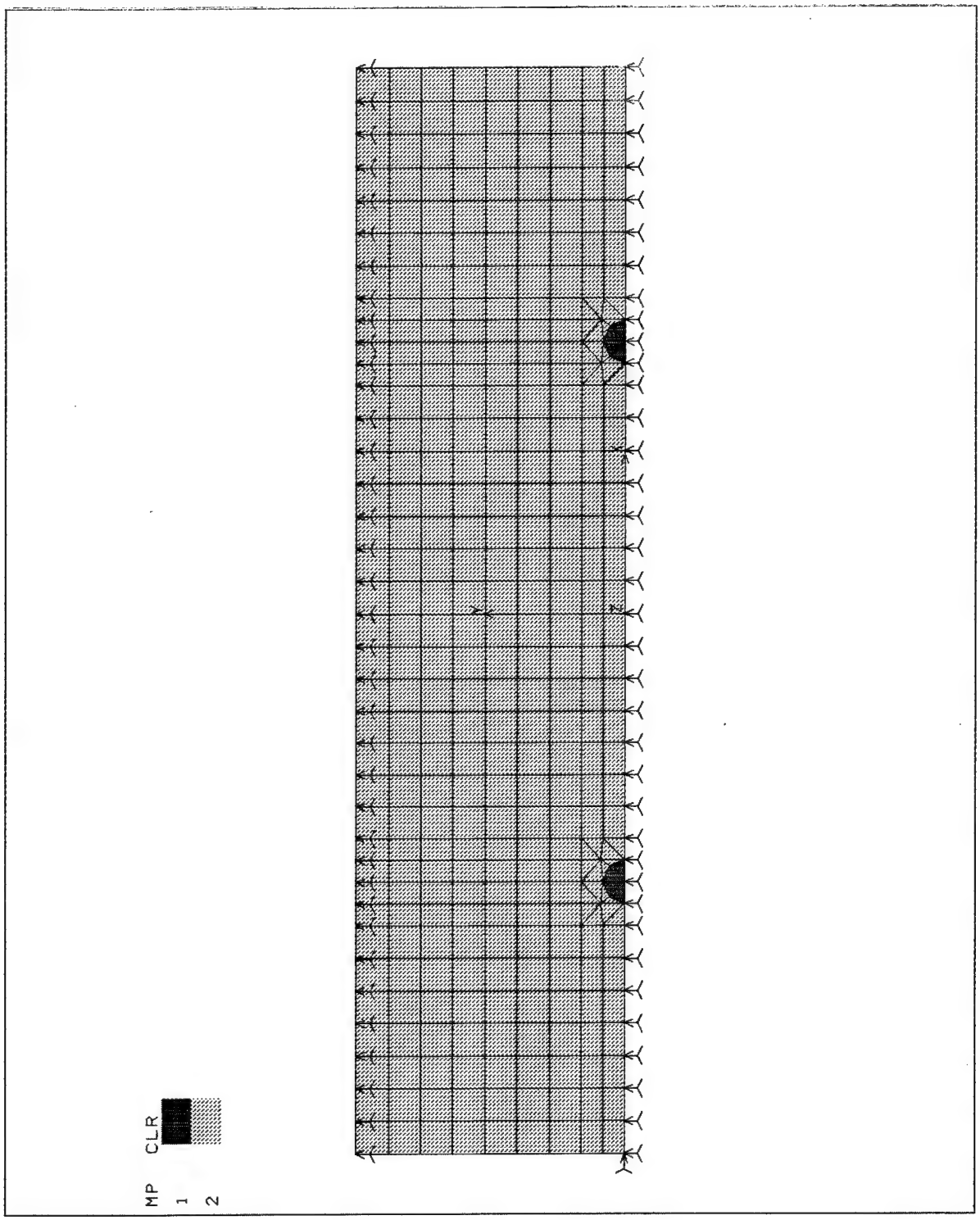

Figure 33 — Boundary Conditions as Viewed from the Positive Z-Axis, Pin Intact

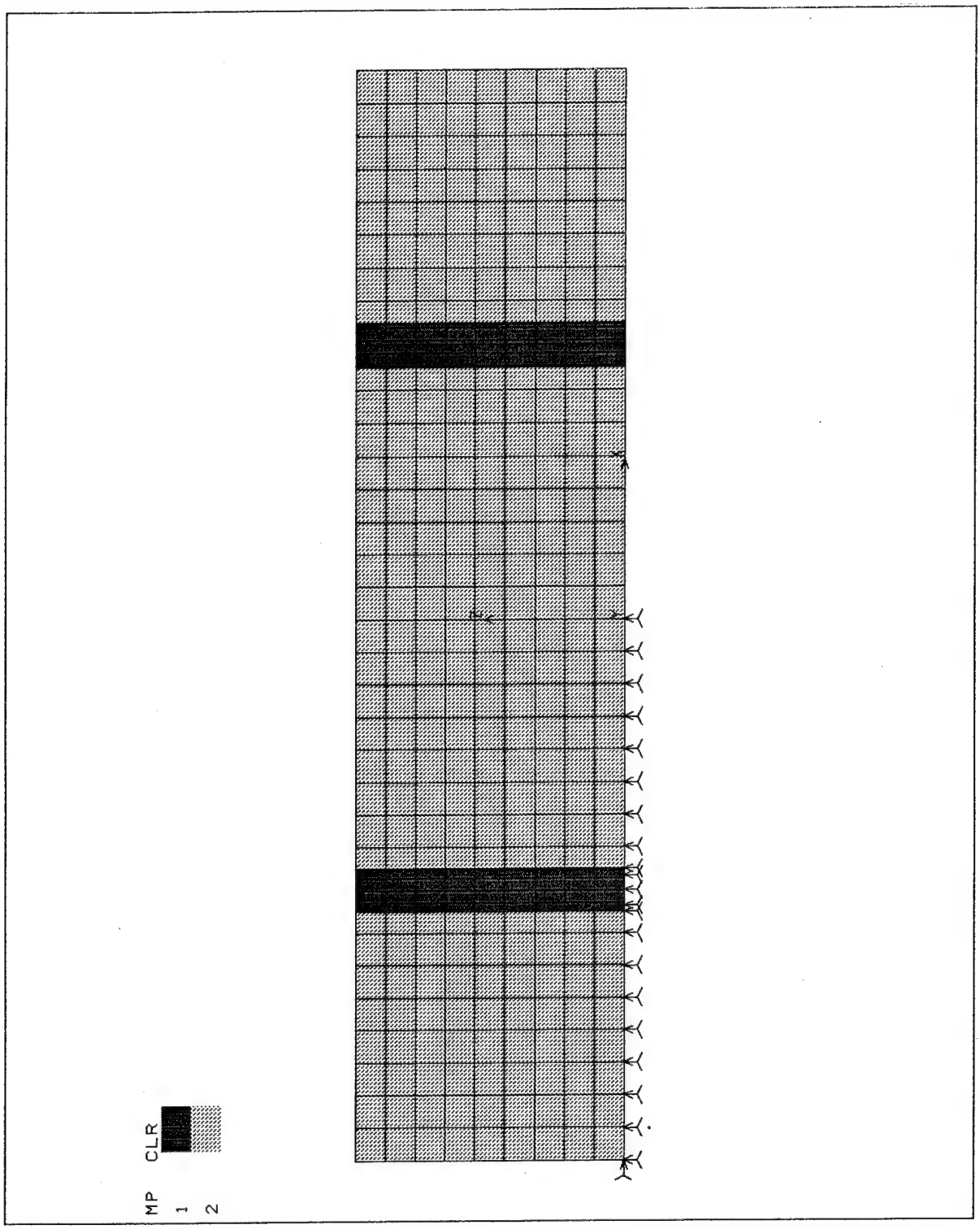

Figure 34 — Boundary Conditions as Viewed from the Negative Y-Axis, Pin Severed

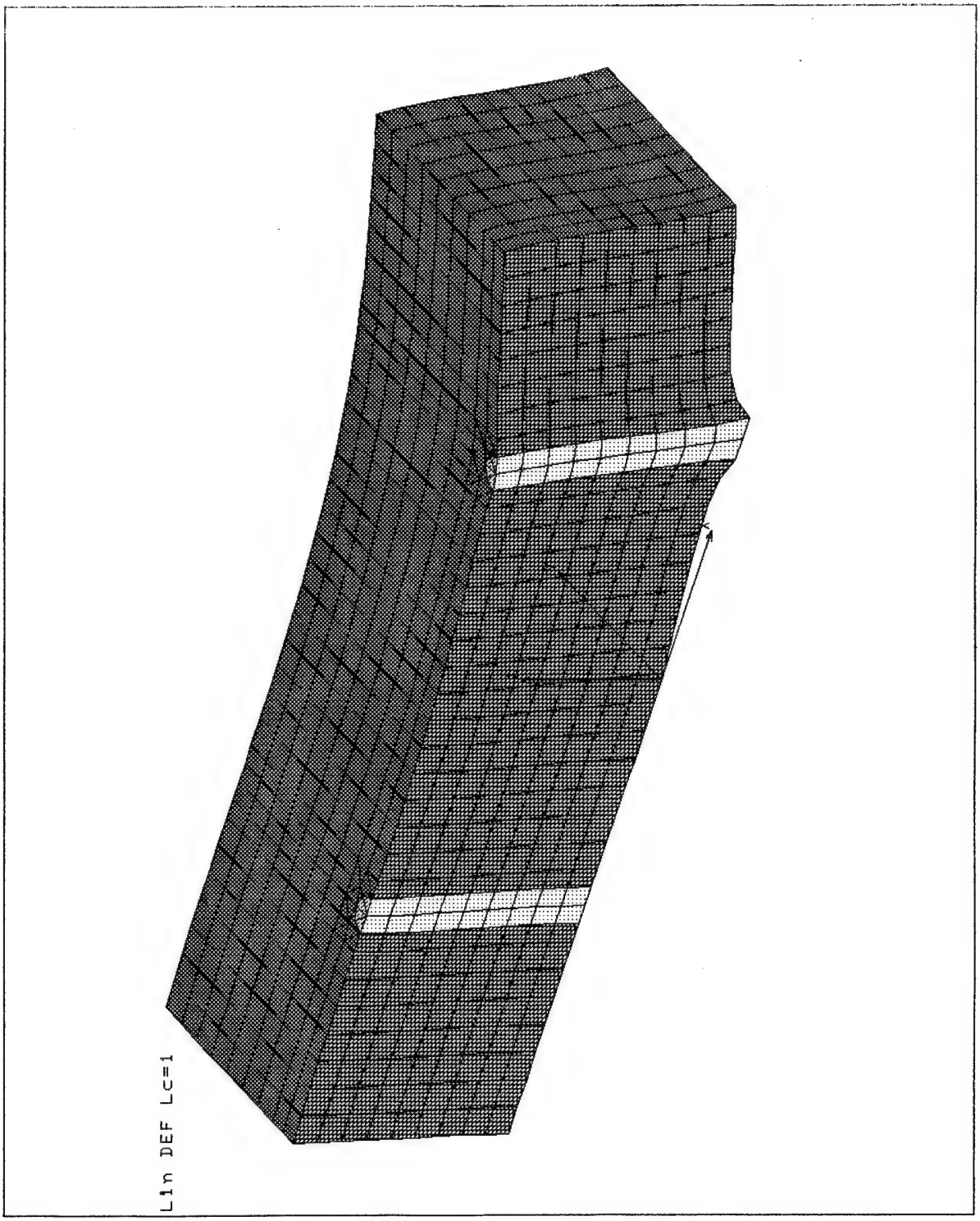

Figure 35 — Displacements due to Crack Opening Loads, Pin Intact

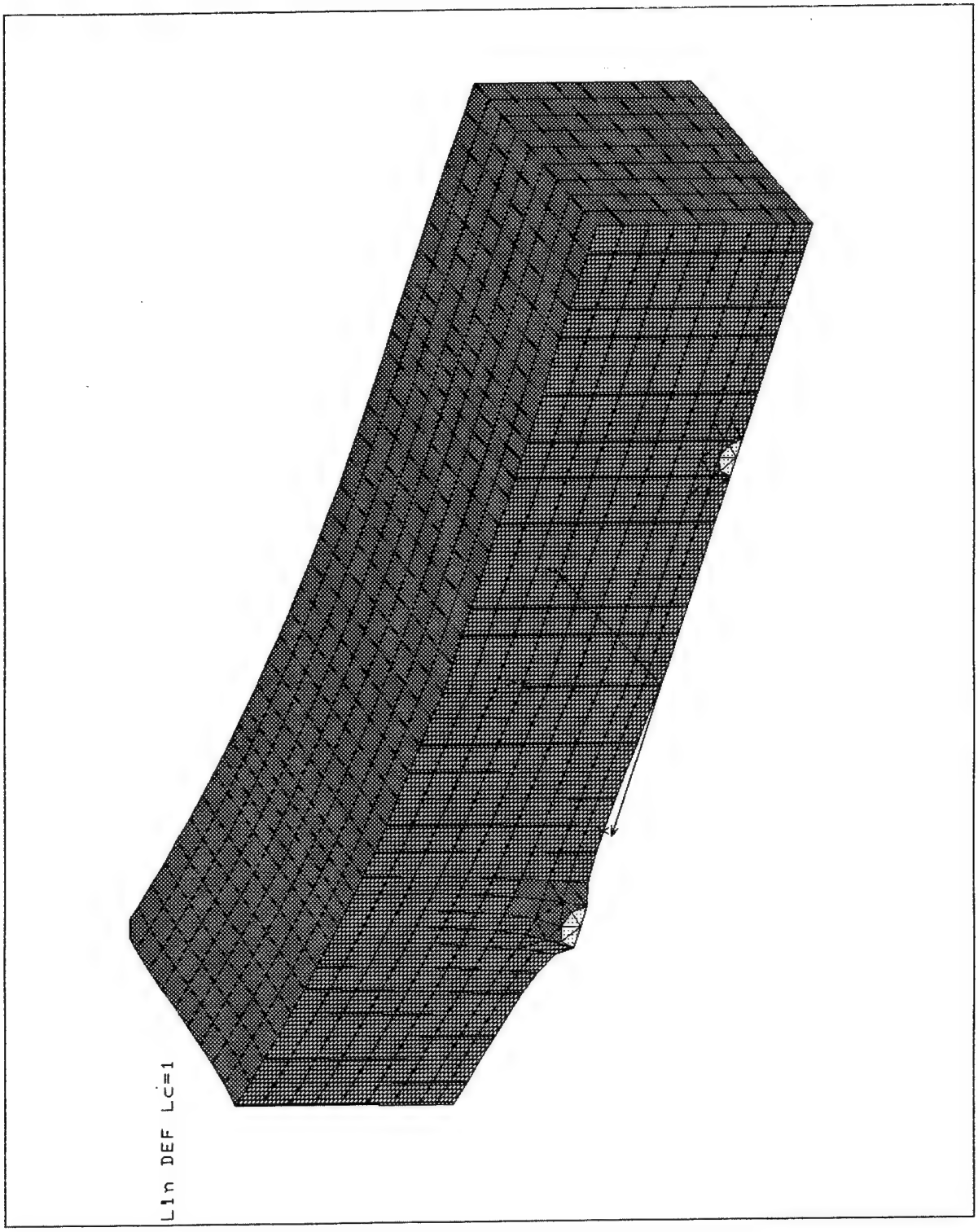

Figure 36 — Displacements due to Crack Opening Loads, View from Crack Side

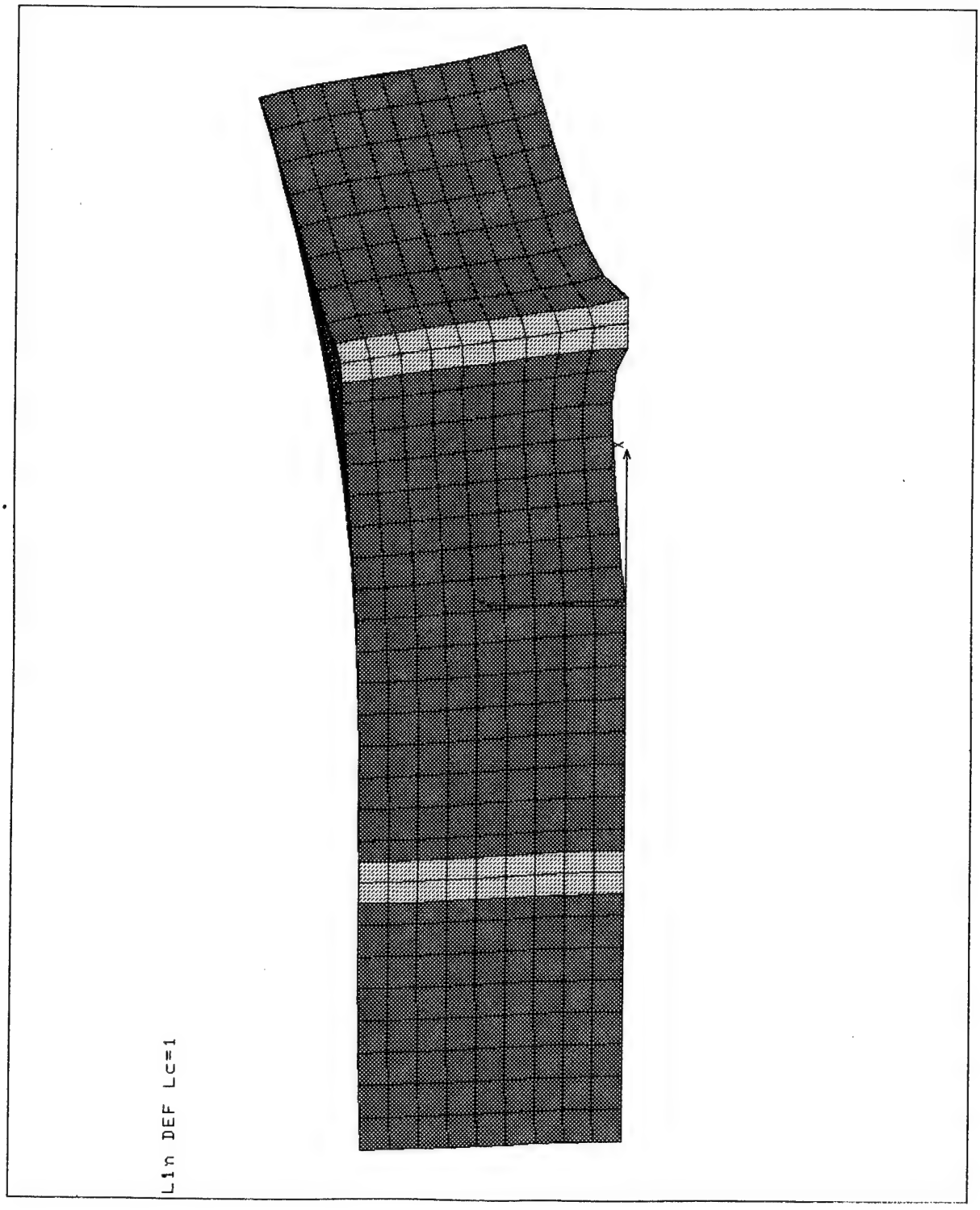

Figure 37 — Displacements due to Crack Opening Loads, Side View

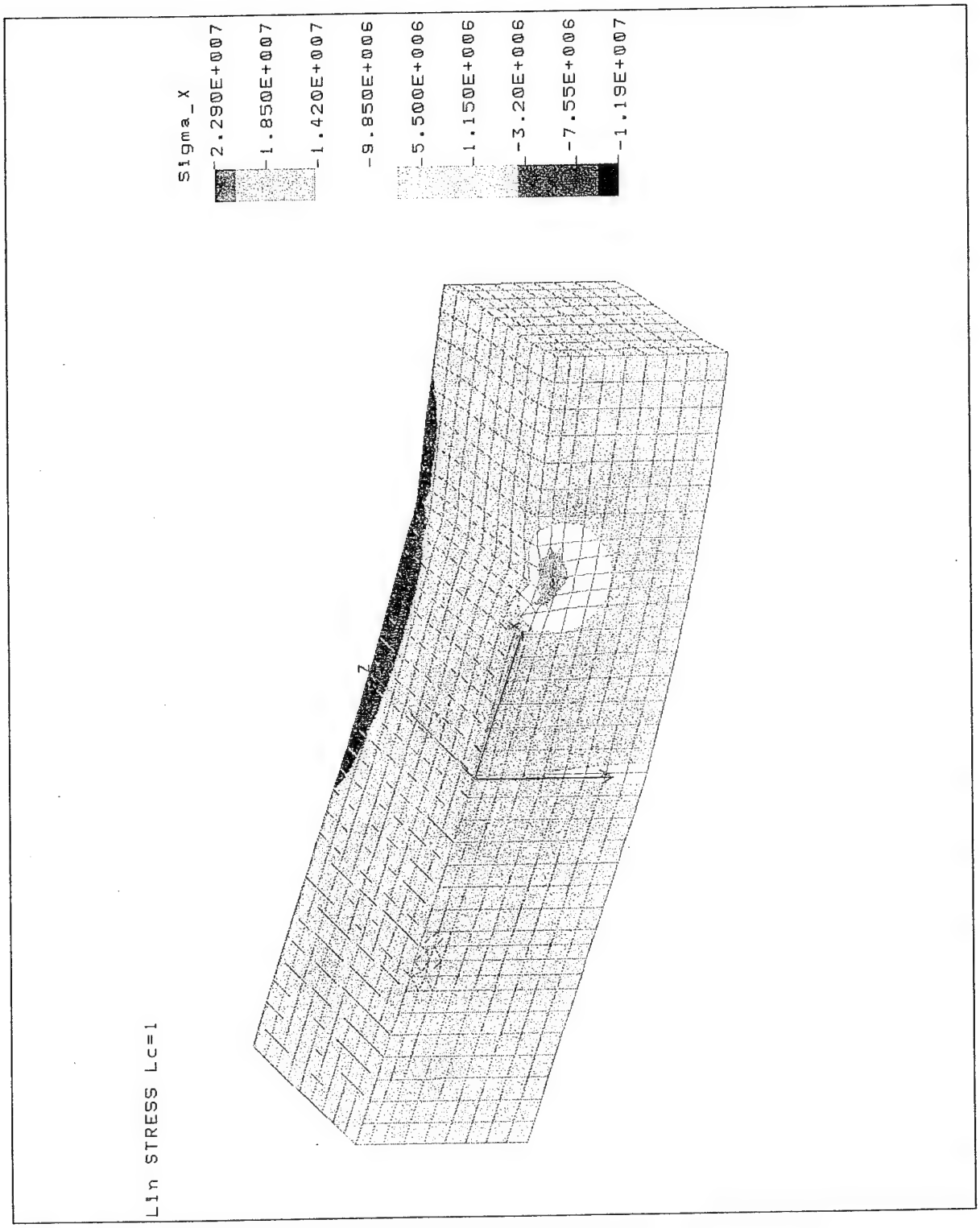

Figure 38 — Bending Stresses (Pa), Pin Intact

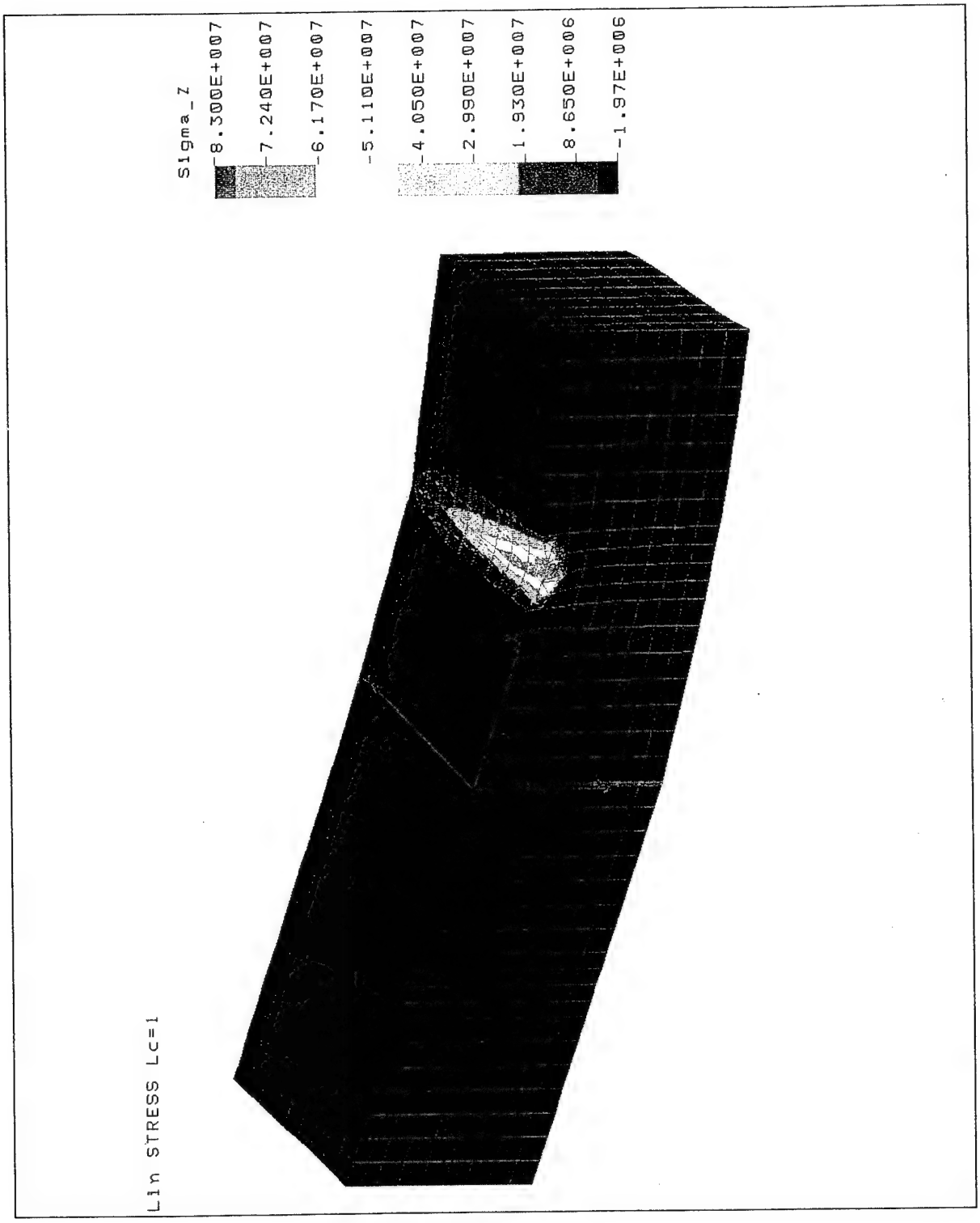

Figure 39 — Through-the-Thickness Stresses (Pa), Pin Intact

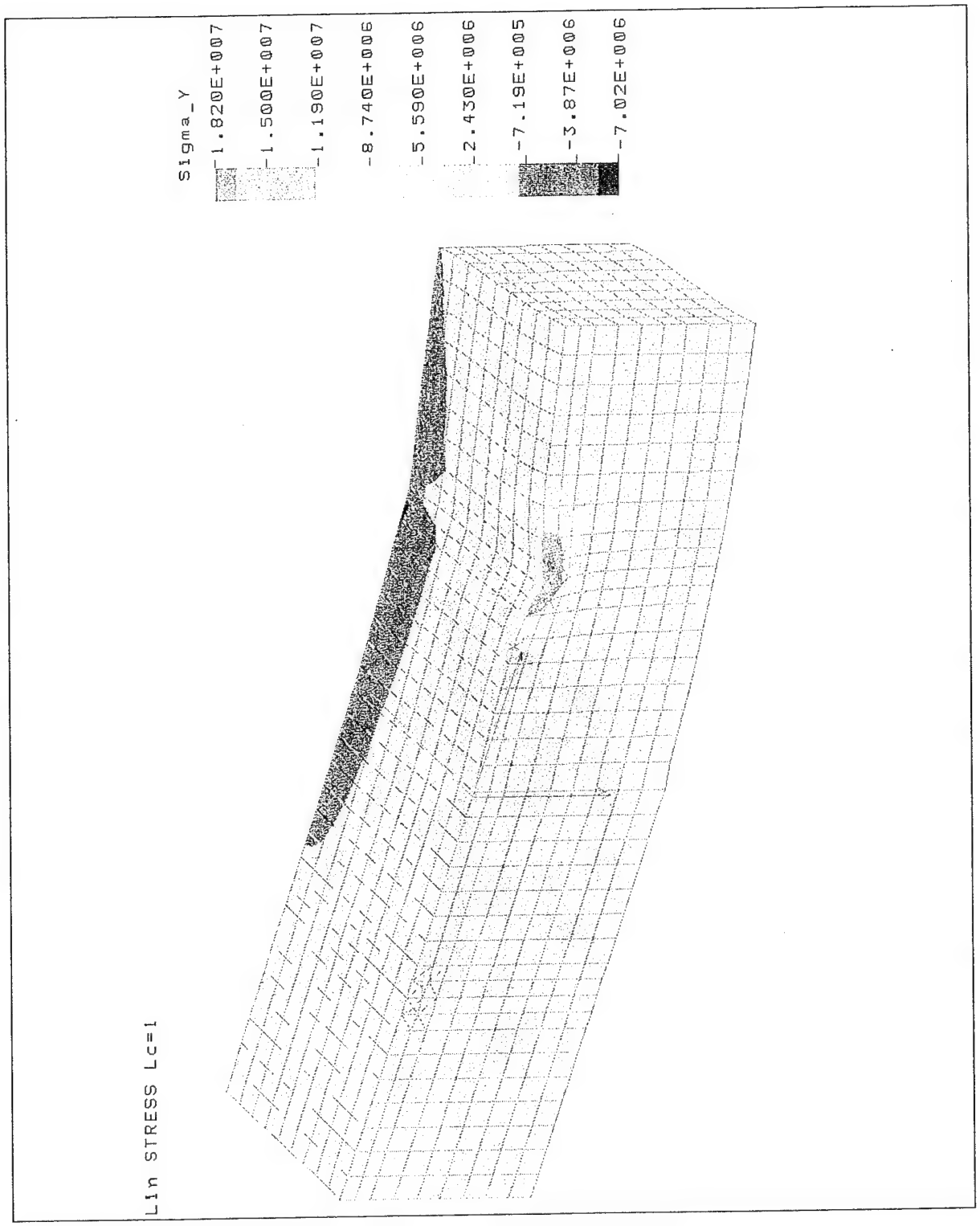

Figure 40 — In-Plane Lateral Stresses (Pa), Pin Intact

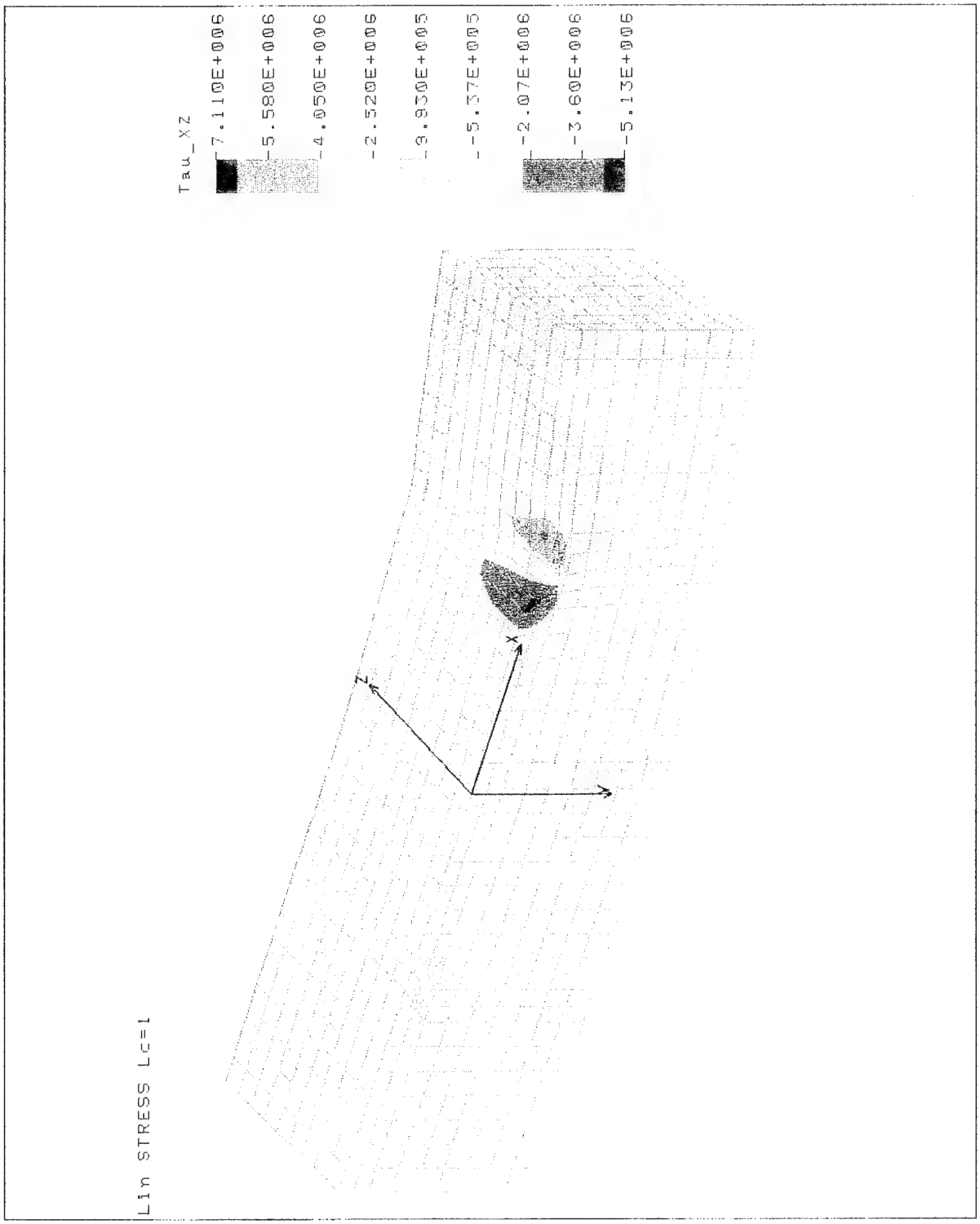

Figure 41 — Shear Stresses (Pa), Pin Intact

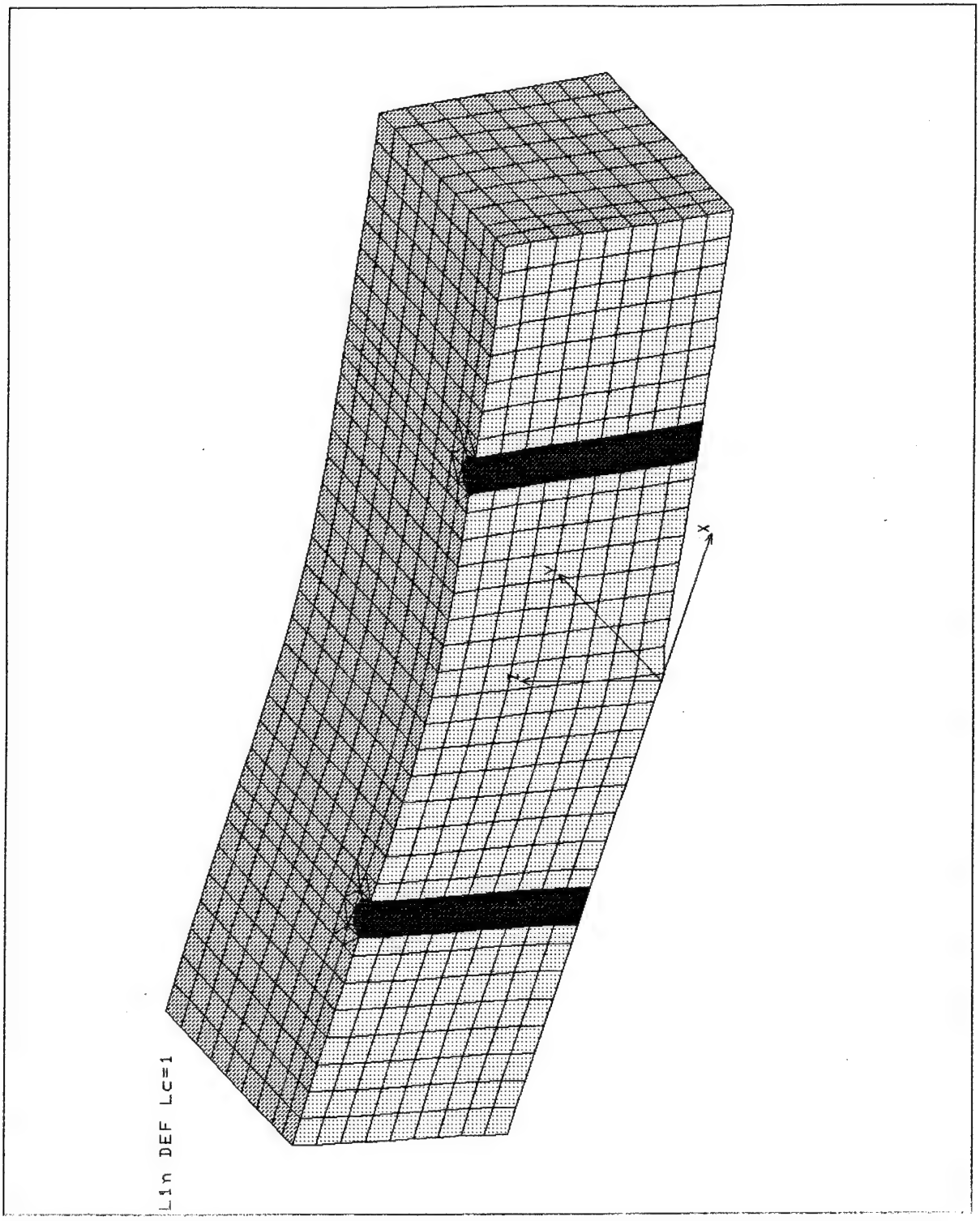

Figure 42 — Displacements due to Crack Opening Loads, Pin Severed

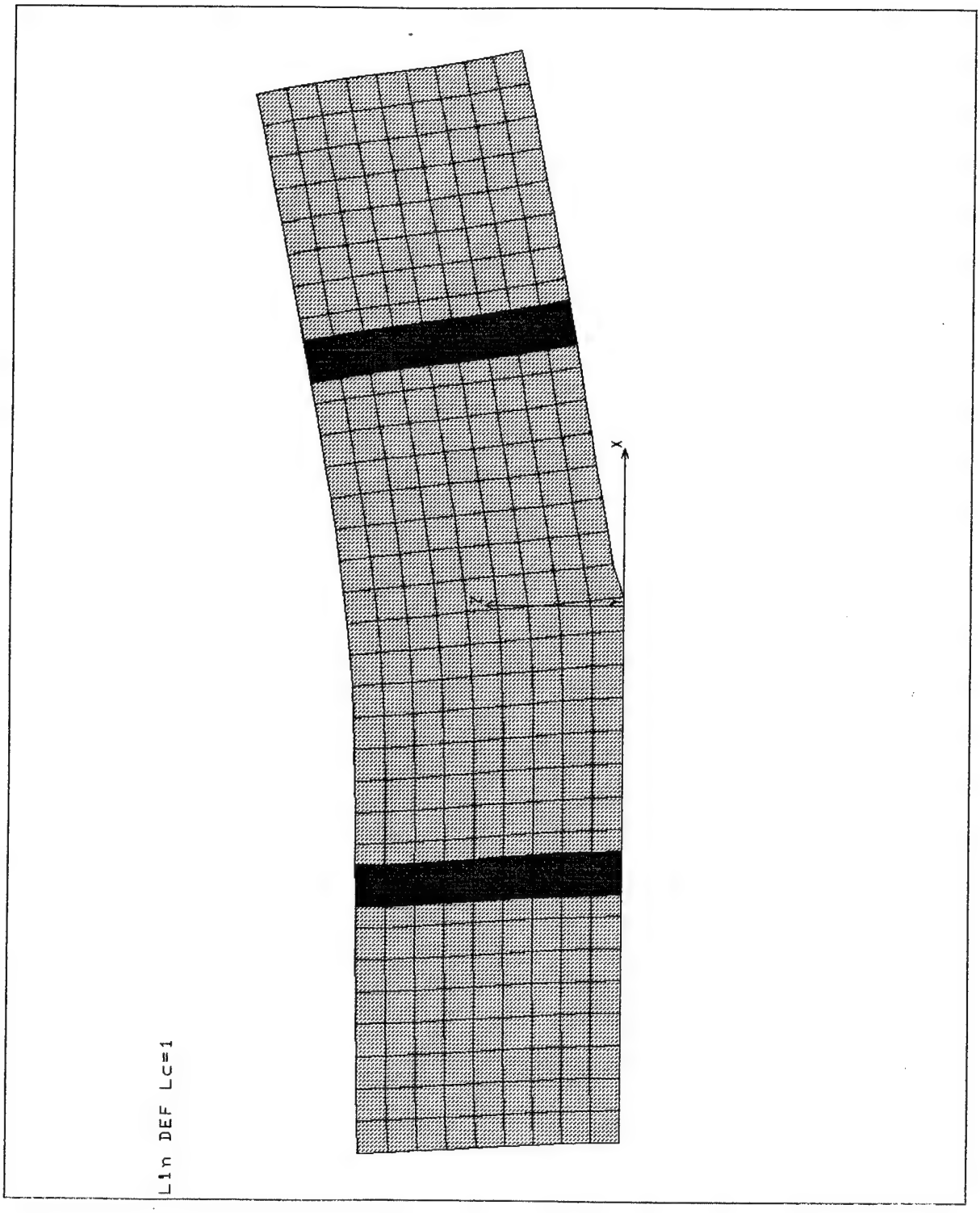

Figure 43 — Displacements due to Crack Opening Loads, Side View

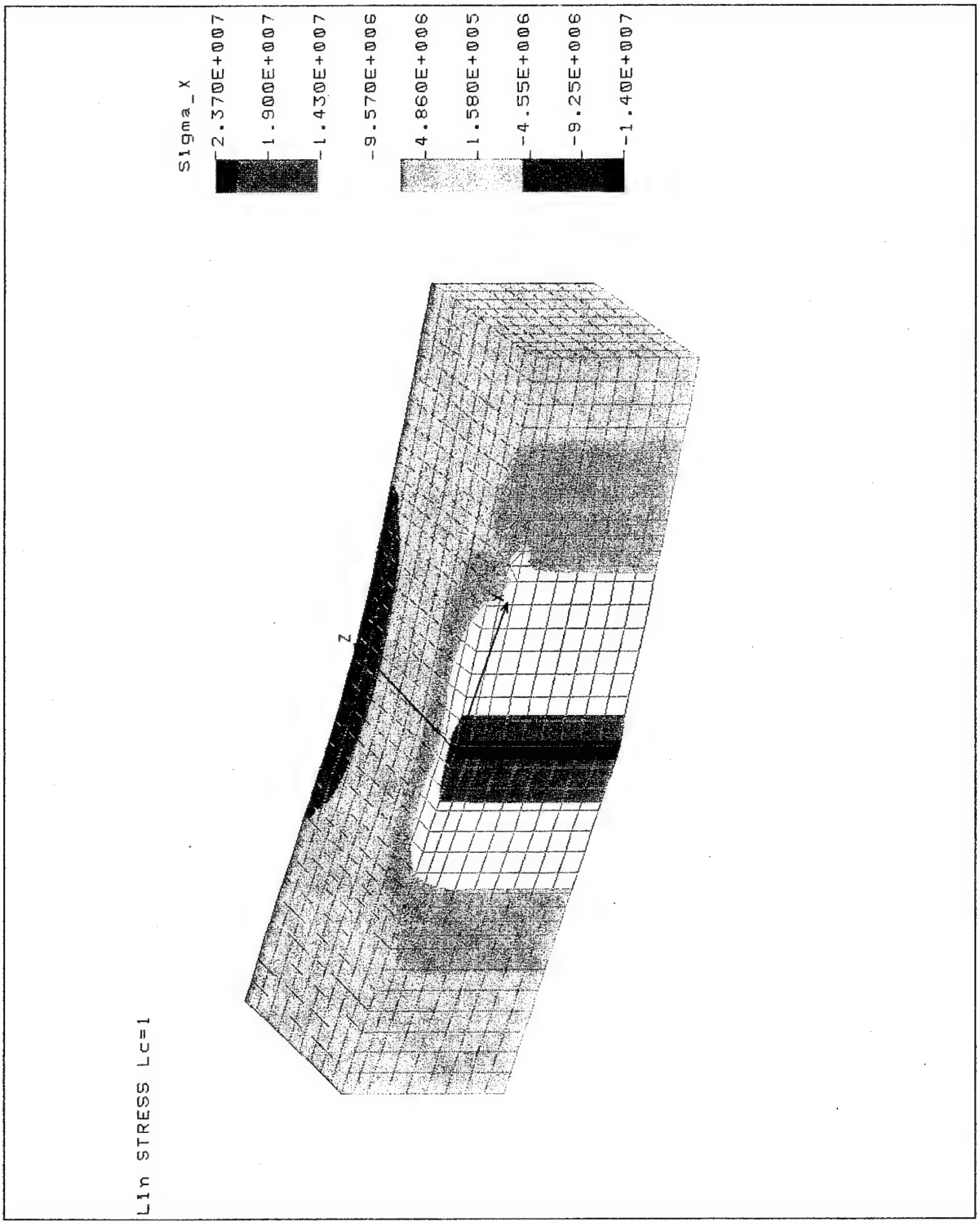

Figure 44 — Bending Stresses (Pa), Pin Severed

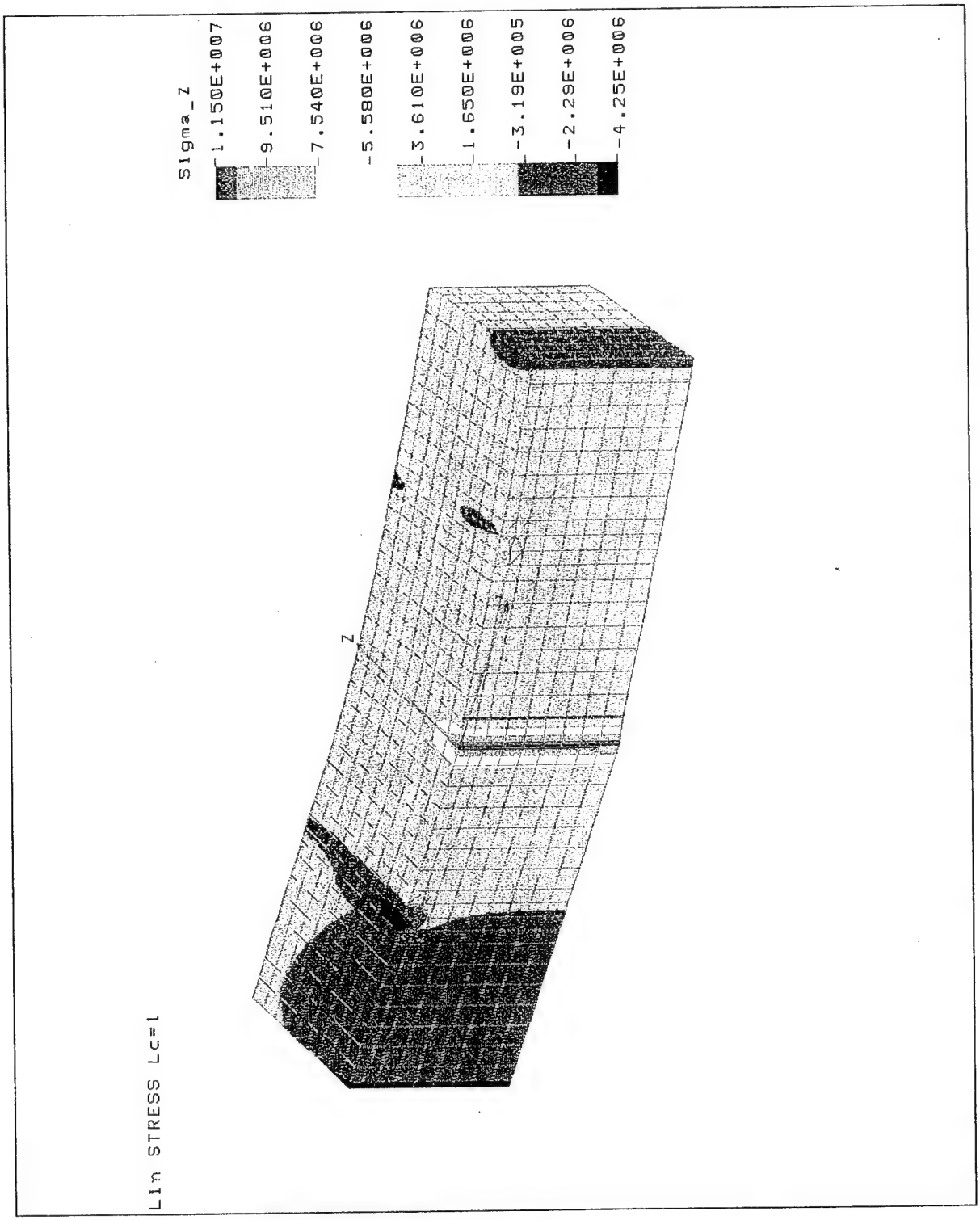

Figure 45 — Through-the-Thickness Stresses (Pa), Pin Severed

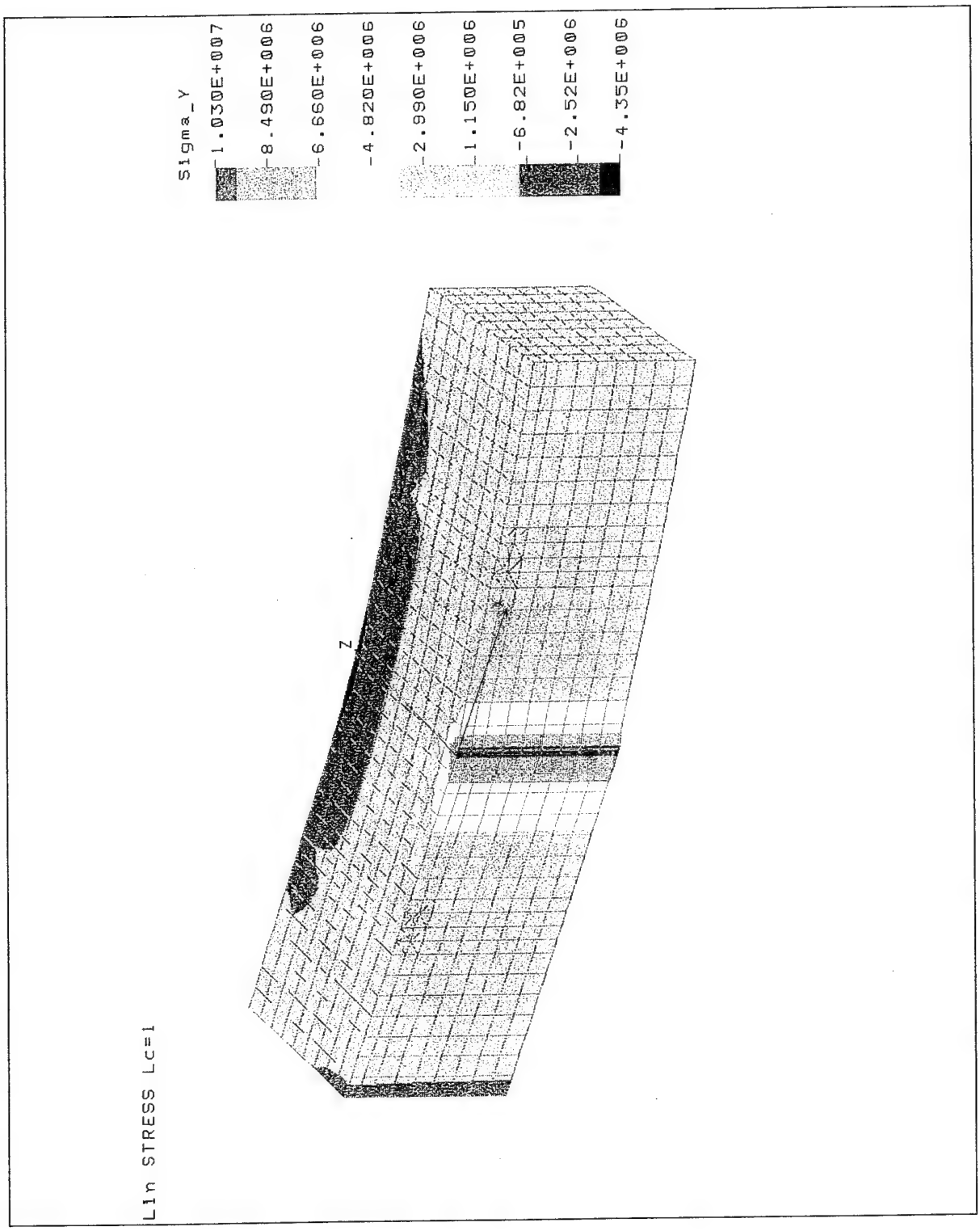

Figure 46 — In-Plane Lateral Stresses (Pa), Pin Severed

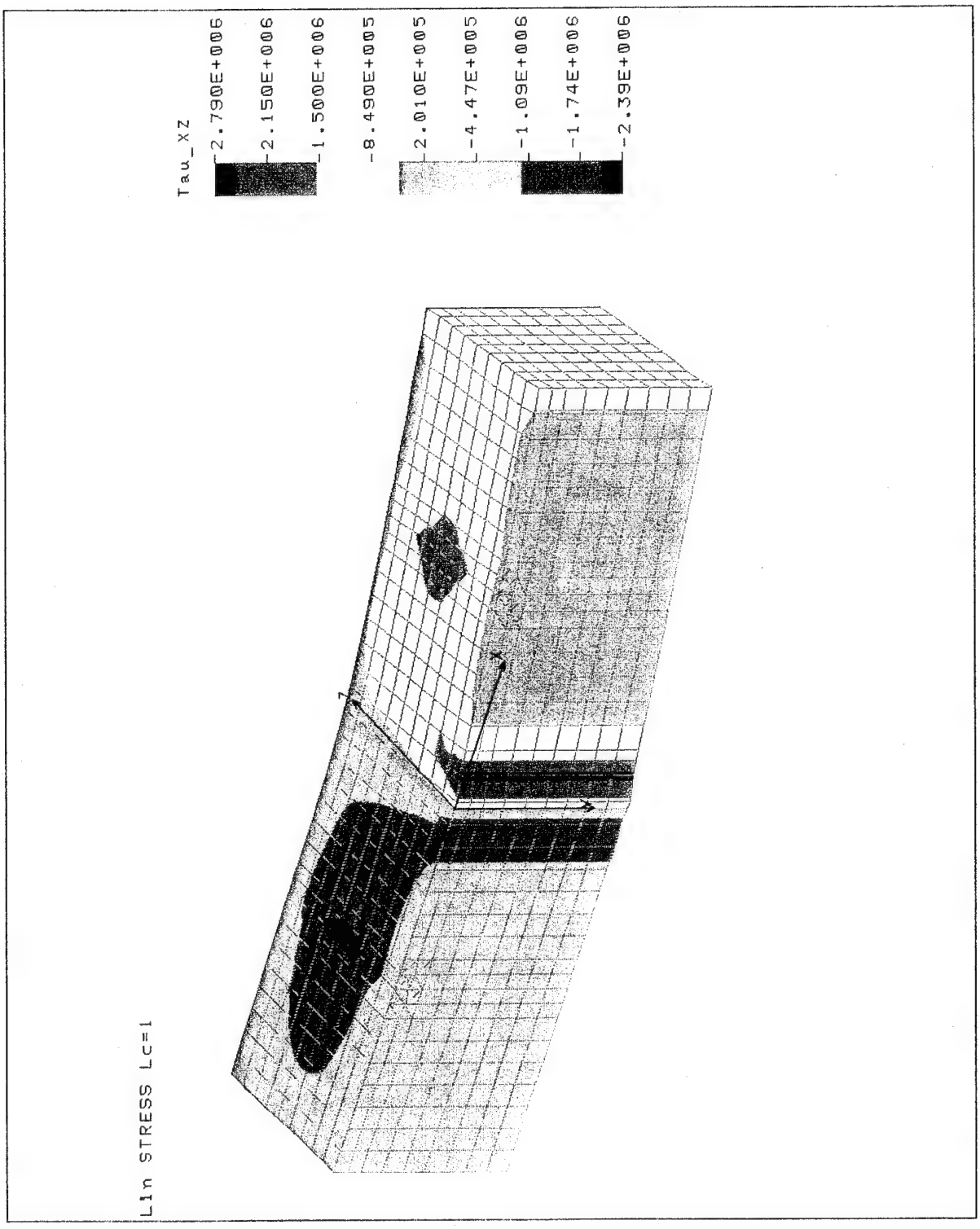

Figure 47 — Shear Stresses (Pa), Pin Severed

DISTRIBUTION LIST

Report No. NAWCADWAR-95-12-TR

No. of Copies

Northrup Grumman Corporation 1
Attn: Technical Library
One Northrup Avenue
Hawthorne, CA 90250

Northrup Grumman Corporation 1
Attn: Dr. H.P. Kan
One Northrup Ave.
Hawthorn, CA 90250

Northrup Grumman Corporation 1
Attn: Fr. Ravi Deo
One Northrup Avenue
Hawthorne, CA 90250

Northrup Gruman Corporation 1
Vought Aircraft Company
Attn: Technical Library
P.O. Box 655907
Dallas, TX 75265-5907

Rockwell International/North American Aircraft Division 1
Attn: Technical Library
P.O. Box 92098
Los Angeles, CA 90009

Rockwell International/North American Aircraft Division 1
Attn: Technical Library
P.O. Box 582808
Tulsa, OK 74158

Sikorsky Aircraft 1
Attn: Technical Library
North Main Street
Stratford, CT 06601-1381

NAVAIRWARCENACDIVWAR 1
Tomm Hess, Code 4.3.3

NAVAIRWARCENACDIVWAR 1
Code 4.3.4
NAVAIRWARCENACDIVWAR 2
Code 7.2.5.5

NAVAIRWARCENACDIVWAR 15
Code 4.3.3.1

NAVAIRWARCENACDIVPAX 2
Attn: Ms. Dorothy Ropper
MS2, Bldg. 405, Code 7.2.2.3A

DISTRIBUTION LIST

Report No. NAWCADWAR-95-12-TR

No. of Copies

Lockheed Martin/Missile and Space Company 1
Attn: Technical Library
1111 Lockheed Way
Sunnyvale, CA 94088

McDonnell-Douglas Aerospace 1
Attn: Technical Library
P.O. Box 516
St. Louis, MO 63166

McDonnell-Douglas Aerospace 1
Attn: Mr. C. Pingle, M/S 0644465
P.O. Box 516
St. Louis, MO 63166

McDonnell-Douglas Aeorspace 1
Attn: Technical Library
Mail Code 36-84
3855 Lakewood Blvd.
Long Beach, CA 90846

McDonnell-Douglas Aeorspace 1
Attn: Mr. J. Goering
Dept. 337, M/S 245-1065
P.O. Box 516
St. Louis, MO 63166

McDonnell-DOuglas Helicopter Company 1
Attn: Technical Library
5000 E. McDowell Road
Mesa, AZ 85205

McDonnell-Douglas Astronautics 1
Attn: Technical Library
5301 Bolsa Ave.
Huntington Beach, CA 92647

Northrup Grumman Corporation 1
Attn: Technical Library
South Oyster Bay Road
Bethpage, Long Island, NY 11714

Northrop Grumman Corporation 1
Attn: Mr. A. Ferarri
South Oyster Bay Road
Bethpage, Long Island, NY 11714

DISTRIBUTION LIST

Report No. NAWCADWAR-95-12-TR

No. of Copies

Boeing Defense & Space Group 1
Helicopter Division
Attn: Technical Library
P.O. Box 16858
Philadelphia, PA 19142-0858

Boeing Defense & Space Group 1
Attn: Mr. J. Howitt, Jr. M/S 4H-79
P.O. Box 3707
Seattle, WA 98124-2207

Boeing Co. Wichita Division 1
Tech. Library K78-38
P.O. Box 7730
Wichita, KS 67277-7730

General Electric Company 1
Attn: Technical Library
P.O. Box 8555
Philadelphia, PA 19101

Great Lakes Composite Consortium 1
Attn: John R. Holland
8400 Lakeview Parkway
Suite 800
Kenosha, WI 53142

Lockheed Martin/Fort Worth Division 1
Attn: Technical Library
P.O. Box 748
Fort Worth, TX 76101

Lockheed Martin/Fort Worth Division 1
Attn: Dr. G. Law
P.O. Box 748
Fort Worth, TX 76101

Lockheed Martin/Georgia Company 1
Attn: Technical Library
86 South Cobb Drive
Marietta, GA 30063

Lockheed Martin/Georgia Company 1
Attn: Technical Information
Dept. 72-34, Zone 26
Marietta, GA 30063

DISTRIBUTION LIST

Report No. NAWCADWAR-95-12-TR

No. of Copies

Administrator 1
National Aeronautics and Space Administration
Lewis Research Center
Attn: Dr. C. Chamis, M/S-49-6
21000 Brookpark Road
Cleveland, OH 44153

Administrator 1
National Aeronautics and Space Administration
Lewis Research Center
Attn: Technical Library
21000 Brookpart Road
Cleveland, OH 44153

Administrator 1
Defense Technical Information Center
Bldg. #5, Cameron Station
Alexandria, VA 23314

Federal Aviation Administration 1
Attn: Mr. J. R. Soderquist, AIR-103
800 Independence Ave., S. W.
Washington, DC 20591

Federal Aviation Administration 1
Attn: Mr. P. Shyprykevich
Technical Center
Atlantic City, NJ 08405

Bell Helicopter/Textron Inc..... 1
Attn: Technical Library
P.O. Box 482
Fort Worth, TX 76101

Bell Helicopter/Textron Inc..... 1
Attn: Mr. D. Reisdorfer
P.O. Box 482
Fort Worth, TX 76101

Boeing Defense & Space Group 1
Helicopter Division
Attn: Dr. C. K. Gunther M/S P30-30
P.O. Box 16858
Philadelphia, PA 19142-0858

DISTRIBUTION LIST

Report No. NAWCADWAR-95-12-TR

No. of Copies

Commanding Officer 1
U. S. Army Aviation Applied Technology Directorate
Attn: T. E. Condon
SAVRT/TY-ASR
Fort Eustis, VA 23604-5577

Commanding Officer 1
Advanced Systems Research and Analysis Office ASRAO
Attn: Library, M/S 219-3
Ames Research Center
Moffett Field, CA 94035-1000

Commanding Officer 1
U. S. Army R & T Laboratory (ARRADCOM)
Attn: K. Abelson
Building 182
Dover, NJ 07801

NASA Headquarters 1
Attn: G. Seidel
OAST-Code RM
Washington, DC 20546

Administrator 1
National Aeronautics and Space Administration
Attn: Airframes Branch, FS 120
Washington, DC 20546

Administrator 1
National Aeronautics and Space Administration
Langley Research Center
Attn: Dr. J. Starnes, M/S 190
Hamptom, VA 23665-5225

Administrator 1
National Aeronautics and Space Administration
Langley Research Center
Attn: Mr. J. Davis, M/S 243/STPO
Hampton, VA 23665-5225

Administrator 1
National Aeronautics and Space Administration
George C. Marshall and Space Administration
George C. Marshall Space Flight Center
Attn: Technical Library
Huntsville, AL 35812

DISTRIBUTION LIST

Report No. NAWCADWAR-95-12-TR

No. of Copies

Attn: Kip Walker
Bldg. 2, Code 351
Jacksonville, FL 32212-0016

Commander 1
Naval Aviation Depot
Attn: D. Perl, Code 343
NAS, North Island, San Diego, CA 92135-5112

Commander 1
United States Naval Academy
Attn: Mechanical Engineering Dept.
Annapolis, MD 21402

Commander 1
U.S. Naval Postgraduate School
Attn: Technical Library
Monterey, CA 93943

Commanding Officer 1
Wright Laboratory
Attn: FIBAC, R. Holzwarth
Wright Patterson Air Force Base, OH 45433-6553

Commanding Officer 1
Wright Laboratory
Attn: FIBAD, L. R. Phillips
Wright Patterson Air Force Base, OH 45433-6553

Commanding Officer 1
Wright Laboratory
Attn: FIBEC Dr. G. Sendeckyj
Wright Patterson Air Force Base, OH 45433-6553

Commanding Officer 1
Wright Laboratory
Attn: FIB, D. Paul
Wright Patterson Air Force Base, OH 45433-6553

Commanding Officer 1
Wright Research and Development Center
Attn: MLSE/T. Reinhart
Wright Patterson Air Force Base, OH 45433-6553

Commanding Officer 1
U.S. Army Air Mobility R & D Lab
Attn: H. Reddick
Fort Eustis, VA 23604

DISTRIBUTION LIST

Report No. NAWCADWAR-95-12-TR

No. of Copies

Commander 1
Naval Air Warfare Center Weapons Division
Attn: K. Bailey, Code 338
China Lake, CA 93355

Commander 1
David Taylor Research Center
Attn: E. T. Camponeschi, Code 2844
Annapolis, MD 21402

Commander 1
David Taylor Research Center
Attn: R. Crane, Code 2801
Annapolis, MD 21402

Commander 1
Naval Aviation Depot
Attn: J. Fuss, Code 4.3.4.4
PSC Box 8021
Cherry Point, NC 28533-0021

Commander 1
Naval Aviation Depot
PSC Box 8021
Attn: K. Workman, V-22 ISST
Cherry Point, NC 28533-0021

Commander 1
Naval Aviation Depot
Attn: T. Price, H-60 ISST
PSC Box 8021
Cherry Point, NC 28533-0021

Commander 1
Naval Aviation Depto — Jacksonville
Structural Materials Engineering
Attn: Jeff Lonergan
Bldg. 793, Code 341
Jacksonville, FL 32212-0016

Commander 1
Naval Aviation Depot — Jacksonville
Structures and Analysis Branch

DISTRIBUTION LIST

Report No. NAWCADWAR-95-12-TR

No. of Copies

Office of Naval Research 5
Attn: W. King, ONT-212
800 N. Quincy St.
Arlington, VA 22217

Office of Naval Research 1
Attn: A. K. Vasudevan, Code 1216
800 N. Quincy St.
Arlington, VA 22217

Office of Naval Research 1
Attn: Y. Rajapakse, Code 1132SM
800 N. Quincy St.
Arlington, VA 22217

Director 1
Naval Research Laboratory
Attn: L. Gause
4555 Overlook Ave., S.W.
Washington, DC 20375-5000

Commander 1
Naval Air Systems Command
Attn: NAVAIR 4.3.3
Washington, DC 20361

Commander 1
Naval Air Systems Command
Attn: NAVAIR 4.3.3.1
Washington, DC 20361

Commander 1
Naval Air Systems Command
Attn: NAVAIR 4.3.3.2
Washington, DC 20361

Commander 1
Naval Air Systems Command
Attn: NAVAIR 4.3.3.3
Washington, DC 20361

Commander 1
Naval Air Systems Command
Attn: NAVAIR 4.3.4
Washington, DC 20361